Nanocoatings

Nanomaterials and Nanostructures Coatings Fabrication Using Detonation and Plasma Detonation Techniques

A.D. Pogrebnjak, S.N. Bratushka, O.V. Bondar, D.L. Alontseva, S.V. Plotnikov, and O.M. Ivasishin

CONTENTS

AQ1

INTRODUCTION

One of the most topical problems of materials science and solid-state physics is the production of nanostructured coatings and films with high protective properties. Among numerous known methods for fabrication of such coatings, one of the most promising techniques is the coating deposition using plasma detonation technique.

The coatings, deposited by plasma detonation method, possess no such limitation,[1,2] and the conditions of their deposition—temperature of the plasma jet—on the order of a few thousands Celsius degrees, high velocities (from 600 to 1000 m/s)[2] of the sprayed particles in the plasma jet, and small time (about 3 ms) of the action of the jet are such that the assumptions on the formation of amorphous regions or nanostructures therein are quite justified. It is also known that amorphous or nanostructured states are obtained especially efficiently at high rates of heating, high pressures, and little time of the action of high temperatures.[3,4] The authors,[5–8] who studied the structure and properties of coatings deposited by a plasma jet, noted the formation of nanostructures therein after electron irradiation. It should be noted that the formation of an ultrafine disperse structure leads to a substantial improvement and (in some cases) to fundamental changes in the properties of the material.[6–8] From the physical viewpoint, the transition to a nanostructured state leads to the appearance of size effects, by which a set of phenomena should be meant that are related to changes in the properties of the substance because of a coincidence between the size of a microstructural block and a certain critical length (domain wall thickness, critical radius of a dislocation loop, etc.) characterizing the phenomena.[9,10]

The authors[11] showed that the Ni–Cr-based coatings with different content of chromium and additions of B, Si, and Fe deposited by a plasma jet with a subsequent partial melting of the surface layer of coatings by an electron beam or by a plasma jet can be used to protect metals (steels) against wear and corrosion and to enhance hardness in comparison with the substrate.[8,11,12]

It is also well known that Ni–Cr-based coatings (Ni–Cr; Ni–Mo–Cr) serve as a good protection from the action of a mixture of acids (HCl, H_2SO_4, HNO_3 + HF_4) upon operation under elevated temperatures.[12–14] Upon usage of protective coatings of these alloys 80–300 μm thick, they can be used fairly long, thereby providing materials with good performance characteristics.[12–14]

The Co–Cr powder coatings produced by plasma detonation technology contain a total spectrum of intermetalloids, and according to the performed investigations, endured high temperatures and loads in aggressive media.[12] However, according to the results,[12–14] plasma detonation treatment of powder coatings have a number of disadvantages such as thin oxide layers in the treated surfaces and pores in the coating (from 0.5% to 1.8%).[15–17] To obtain the lesser porosity of the powder coatings and to improve cohesion and adhesion properties on the interface of coating substrate, in practice, the coating surface is melted by pulsed plasma jet and electron beams of high energy density.[8,11,16,17] Treatment of a solid surface by concentrated energy fluxes reduced to absorption of some part of the incident energy, which activated various physical and chemical processes on the surface layer and through the coating depth (heating, melting, cooling, changes of the surface phase, plasma chemical reactions, intensification of practically all diffusion mechanisms, etc.).[5,7,9,11,17,18] An important

AQ2

advantage of the pulsed plasma surface modification is its possibility to saturate the near-surface coating layers by refractory doping elements. It is known[8,11,18–20] that mechanical, physical, and chemical properties of coatings fabricated by plasma detonation depend on a near-surface region relief, as well as on their component and phase composition, and their corrosion resistance depends on the concentration of pores.[17–19] To avoid porosity, for instance, we can seal various nonuniformities of the coating and increase adhesion power between a coating and a substrate. The improvement of mechanical characteristics of the treated surfaces is possible either by changing the surface phase composition or by enrichment of the coating near-surface layers by refractory elements as a result of ion doping or surface melting by pulsed plasma jet. According to the performed investigations of morphological properties of the surfaces after its treatment by high-velocity plasma jet (HVPJ), we can see the essential smoothing of its relief and decreasing of the degree of the coating surface roughness. However, some particles (depending on its initial size), being treated by HVPJ for the second time, did not melt.

According to the scientific literature, the technology of plasma detonation deposition of powder coatings consists of two main stages:

(a) Careful preparation of a surface before deposition (cleaning and thermal activation)
(b) Powder deposition onto the substrate surface by pulsed plasma jet[18–21]

It is well known that coatings, based on Ni–Cr–Fe(B, Si), are widely used in reactor building industry.[18,22] Coatings, based on (Co–Cr), which different modifications are known under the common term "Stellite," can be used for mechanical protection of turbine blades in power engineering (hydropower plants, nuclear power plants, etc.). Therefore, the creation of coatings of such type and investigation of their properties appears to be an important task for modern power machine material science.[9,10,17,19,23,24]

In light of the above, the aim of the present work is to study the structure and properties of powder materials (Co–Cr based), deposited on the steel substrate using high-velocity plasma detonation jet, in the case of coating's surface layer melting. Also, it is important to fabricate and investigate coatings based on Ni–Cr with high physical and mechanical properties and with the high level of corrosion resistance to the aggressive media. AQ3

METHODS OF SAMPLE MANUFACTURING AND ANALYSIS

The coatings with the thickness of 80, 120, 150, and 200 μm were deposited by spraying Co–Cr powder with a cobalt base with the nominal composition: Cr (8%–32%), Ni (≤3%), Si (1.7%–2.5%), Fe (≤3%), C (1.3%–1.7%), and W (4%–5%) on the steel substrate using the plasma detonation device "Impulse-6" (Paton Welding Institute).[2]

In this chapter, we use the Impulse-6 device, the principles of work of which are described in the following text. These techniques are based on electromagnetic acceleration of the products of premixed gas combustion.[1,25–32] It was proposed [2,11,14,16] to use a special chamber (1 in Figure 1) for gaseous mixture preparation and detonation. The chamber is

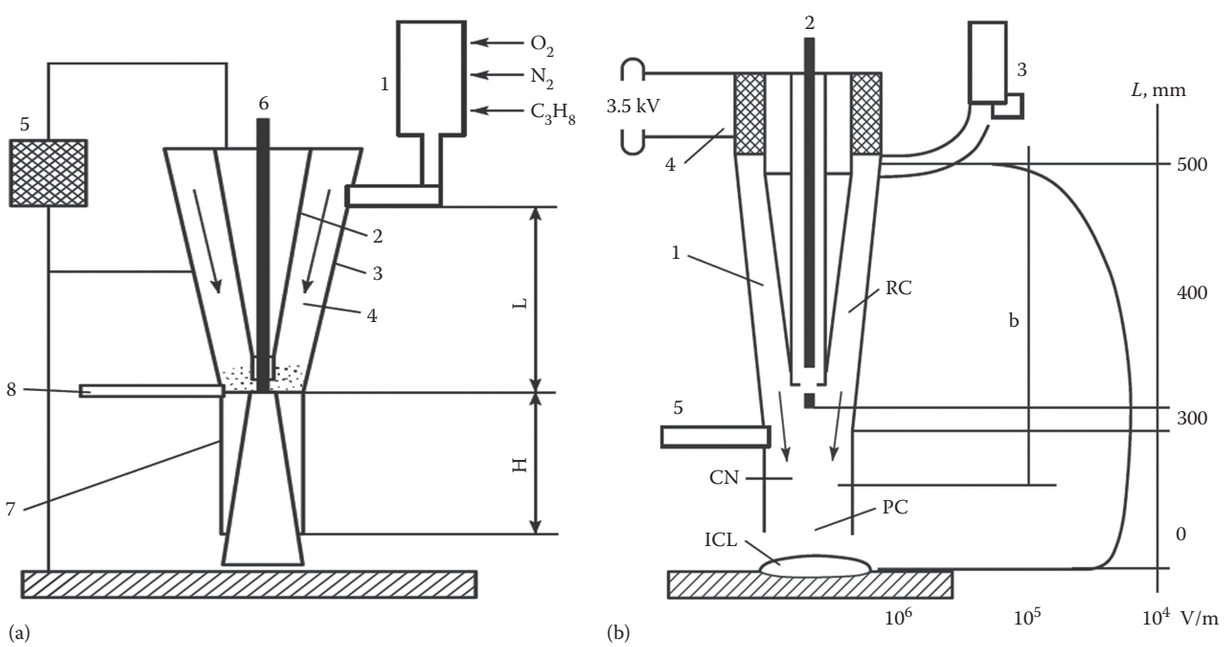

FIGURE 1 Schematic of a pulsed jet plasma spray facility based on an electromagnetic principle of additional energy input: (a) design of the pulsed plasma spray gun and (b) profile of electric field strength. (From Tyurin, Yu.N. and Pogrebnjak, A.D., *Surf. Coat. Technol.*, 111(2–3), 269, 1999.)

separated from the plasma gun. The plasma gun consists of an inner conical electrode (2) and an outer cathode (3). In the annular gap of length L (4) between the coaxial electrodes, an electric field of intensity E is generated by means of a high-voltage source (5). The central electrode holds an expendable metal rod (6). A typical rod is made of a refractory metal or alloy. The plasma gun has a barrel (7), in which the powder is heated and accelerated. The barrel length H depends on the elemental composition and size distribution of the powder. When a hard alloy is deposited, H = 300 mm. The powder is injected into the barrel through a tube (8).

The gaseous mixture components are fed into the detonation chamber (1). Their mixing is followed by the initiation of a detonation. Then, the burned gas flows out of the detonation chamber into the electrode gap (4) and closes the circuit containing the voltage generator (5). The conductive layer of combustion products is accelerated by gasdynamic and electrodynamic forces. The powder injected into the barrel (7) is heated and accelerated by the plasma jet. The heated expendable metal rod (6) evaporates and supplies an alloying element to the plasma jet. When ejected from the plasma gun, a plasma jet closes the electric circuit between the electrode and coated surface as anode and cathode, respectively. The current carried by the jet generates a magnetic field pulse, while the plasma and powder are further heated through the Joule heat release.[33–38]

Selection of deposition regimes of Ni–Cr and Co–Cr coatings were based on numerical evaluation of plasma jet influence on the coatings using thermal conduction equation, taking into account phase transformations and different thermodynamical characteristics of powders.[13,17,18] Due to obtained numerical data and theoretical evaluations, we got plasma jet velocity, temperature, and velocity of powder mix, and we use these data in the present work.

The size of the Co–Cr powder particles was from 56 to 87 μm. The size of the substrate samples was 20 × 30 × 2 mm, and these substrate samples were preliminarily subjected to sand-blasting treatment. Plasma detonation powder materials were deposited in the case of such parameters: the distance from the sample to the plasmatron (detonation gun for deposition) nozzle was 60 mm, a velocity of sample motion was 360 mm/min, frequency of pulsed iteration was 4 Hz, powder feed rate was 1296×10^3 kg/h, power of a capacitor bank was 800 μF, propane, oxygen and air were used as combustion and plasma-forming gases. We chose Mo as the material of the doping (eroding) electrode. After cooling of the samples in the plasmatron chamber, half of the samples were covered, and another set of samples with coatings was subjected to plasma jet melting one, two, or three times. The surface layer of the coatings was partially remelted by a powder-free plasma jet, with the 45 mm distance from nozzle to sample surface. The feed velocity of the sample was 30.0 m/h in this case.

Operation regimes of the gun were the same as in the case of the deposition; however, the pulsed repetition frequency was 2.5 Hz. The samples were firstly divided into pieces and then subjected to different tests.

To obtain the samples, as the base, a tool steel was used: St3 (C, 0.25%; Si, 0.37%; Mn, 0.8%; P < 0.45%; Fe for balance). Coatings of the thickness of 80, 120, 150, and 200 μm were deposited using an Impulse 6 device with the following operative parameters: powder consumption, ~1.44×10^3 kg/h; pulse repetition, 4 Hz; and the capacity of a capacitor banks, 800 μF. The distance to a sample was 55 mm, and the feed velocity of samples was 22.8 m/h.

To deposit coatings, a Ni–Cr powder (Cr, 8%–14%; B, ~2%; Si, ~2.5%–3%; Fe > 5%; Ni for balance) was used. Powder particles size, used for the coating deposition, was from 28 to 58 μm. Tungsten was employed as the material for the electrode, and WC was used as the eroding electrode. The thickness of the obtained coating was 120, 150, and 200 μm.

For repeated melting (treatment) of the coating, we used alloying (eroding) Mo electrode in both cases.

The surface morphology was studied by means of the scanning electron microscopy (SEM) with reflected and secondary electron modes, using a SEM REMMA-103-01, (SELMI, Sumy, Ukraine) and optical profiler VEECO WYKO NT 1100 (AZ 85706 USA). To determine the chemical composition, an energy-dispersive x-ray spectroscopy (EDS) was applied. The surface phase composition was analyzed by x-ray structure analysis using an x-ray diffraction (XRD) device DRON-2 (St. Petersburg, Russia) in $Cu_{K\alpha}$ emission under conditions of Bragg-Brentano geometry. The diffraction patterns were taken by performing x-ray scan in the range of 2θ angles from 20° to 100°. Diffraction peaks were interpreted with the help of the reference book and a database PCPDWIN.[39]

Through-the-thickness phase composition of the coatings was analyzed using D8Advance (Bruker AFS, Germany 2000). In our work, we used small angle x-ray scattering on small angles 0.5°, 1°, 2°, 3°, 6°. To obtain information about phase composition along the depth using XRD and transmission electron microscopy (TEM), we cut foils from the upper layer of the coating, from the middle layer, and from the transition layer between coating and substrate.

Using JEM-2100 (JEOL, Japan) with the help of TEM methods, we conducted the final investigation of the coatings under the accelerating voltage 200 keV. The investigations of coating surface structure were held using the SEM methods on JSM-6390LV (JEOL, Japan) with add-on for energy-dispersive analysis INCAENERGY (Oxford Instruments, United Kingdom).

For composition of elements of the coatings and substrates, we used the fluorescent x-rays spectral analysis using x-ray spectrometers JSX-3100RII (JEOL, Japan) and JPS-3010MC (JEOL, Japan).

For obtaining complete information about the coating's elementary composition, the scheme of Rutherford backscattering spectroscopy (RBS) was used (on H^+—2.012 MeV and He^+—2.035 MeV and E_p = 2.04 MeV, scattering angle 170°, for normal influence of probing ions on the samples, the detector energy resolution is 16 keV). For interpretation of RBS spectra, measurements of element profiles in depth, the standard program (SIMNRA) was used.

On several samples with coatings, where Fe concentration was enough for analysis, we provide transmission investigations using Mössbauer spectrometry and using

conversion-electron Mössbauer spectroscopy. Thin foils for such investigations were prepared from coatings.

Microhardness measurements of powder coatings, produced by plasma detonation, were performed using PMT-3 (St. Petersburg, Russia) device with a diamond Vickers's pyramid under indenter load 10, 25, 50 g. Nanohardness tests were performed by a three-side Berkovich indenter of a nanohardness device nanoindenter-II (United States). These tests were performed in the following way: first, loading till 10 mN, then holding for a period of 20 s, then the load was decreased up to 80%, under a constant load for a period of 30 s to measure a heat drift, and finally we applied full indenter loading. To determine hardness and elasticity modulus under maximum loading of the indenter, we used methods of Oliver and Pharr.[40] Wear resistance tests were performed using the device SMTs-2 (Kiev, Ukraine) according to the setup "plane cylinder" in a medium of technical vaseline. A criterion for evaluation of friction performance was the material volume ablated in the friction zone. The bulk wear was measured by microweighing after every 800 cycles. The total number of rotations (a counter body or an engine) was about 10^4.

Friction tests were done using tribometer TAU-1M; as a test method, we choose "finger-surface" method in conditions of dry friction. Friction ratio and wear resistance of coatings were defined using reciprocal sliding under room temperature (22°C ± 1°C) and relative humidity 80% ± 5%. Speed of moving of table with a sample was 4 mm/s; rounded indicator was made of hard alloys WC–Co (8%), hardness HRC 87.5, indenter-rounded radius was 0.5 mm, loading on indicator was 1N.

As deposited, samples with coatings were polished before investigations (at first we grinded off surface layer of the thickness (30 ÷ 35) ± (3 ÷ 5) μm). For samples, which had been already treated by plasma jet (two passes), we grinded off surface layer of the thickness not higher than 20 μm, than we polished it and choose best parts for comparing.

Corrosion resistance tests of a modified coating were performed using a Bank-Wenking Potentio-Galvanostat PGS 81R and cells Princeton Applied Research corrosion test. The tests were performed in sulfuric acid solution 0.5 M under temperature up to 80°C. Potential from 1 to 1.3 V was applied to the device electrodes. In all cases, the samples surface exposed to the corroding medium was 1 cm^2.[17–19] The tests in 0.5 M H_2SO_4 solution were carried out in the potential range from −1000 to + 1500 mV in the case of an ambient temperature. By one slow scan (scan rate = 0.25 mV/s), corrosion tests were performed.

The aforementioned experimental conditions were also applied for corrosion tests in HCl and NaCl solutions, whereas the scanning region was from −300 to +1700 mV and from −1000 to 1000 mV, respectively.[18] Slow scans lead to predictions of the general corrosion behavior of material.

We should mention, that some samples with coatings were explored during 1 year (using all methods of analysis), but other samples were explored after 5 and 7 years since forming, and these samples were stored under different weather conditions. But we did not find noticeable differences in results; it will be shown further in the chapter.

RESULTS AND DISCUSSION

As it is seen from the data of coating surface structure analysis using SEM with a microanalysis, after melting, the relief becomes smooth. SEM analysis and that with an optical microscope for the transversal cross sections of the resulting coatings demonstrated that they had no practically pores. An interface between the substrate and coating has a wavy character, that is, there was an observed partial particle implantation into the substrate surface, powder particles being deformed. The interface join does not contain big oxide particles, and some substrate regions get also deformed. Surface preparation seems to have a strong effect, that is, in the process of jet-abrasive treatment, some "peening" is formed in the surface and later is increasing. Additionally, we performed a microanalysis over the depth of transversal cross section of the coating both at a melted and at a nonmelted coating region.

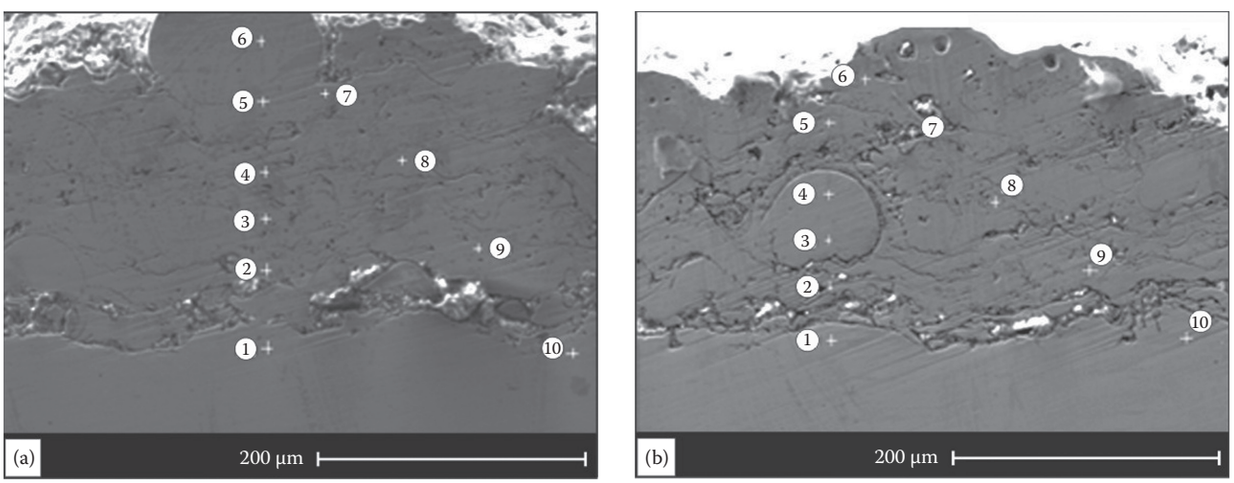

FIGURE 2 Scheme of element analyses for the coatings over their transversal cross sections (coating substrate): (a) an initial coating after pulsed plasma jet deposition (200 μm coating thickness) and (b) after subsequent plasma jet melting (two passes, 200 μm thickness).

Figure 2a and b shows the scheme of analysis over the region depths. As it is seen, the first point turns out to occur not in the melted region but in the substrate. Therefore, there we found a different composition, namely, 90% Fe, 6.72% C, 0.77% Mn, 0.97% P, 0.21% Cr, and 1.96% Al. At the second point, one can observe a sharp increase in the concentration: about 68% Ni; till 10.8% Cr; about 3.25% Si; about 8.27% C; about 1.28% Mo; about 5.78% Fe.

At point 6 near the coating surface (nonmelted), we found about 0.77% C, about 2.91% Si, about 5.18% Fe, about 77.8% Ni, about 12.18% Cr, less than 1% of Mn, and C. At point 10 (again the substrate), we found about 98.5% of Fe, about 0.69% Mn, about 0.49% Ni, and about 0.2% Cr.

The effect of penetration of Ni and Cr into the substrate was observed in all coatings after plasma jet treatment (Figure 2b, Table 1).

From Figure 2b and from Table 1, we can also observe that Fe penetrates from substrate to coating due to pulse plasma treatment (melting).

Thus, acceleration of diffusion processes in the treated samples is confirmed experimentally. Besides the physical characteristics of the treated materials (density, specific thermal capacity, heat conduction, shift modulus, etc.), the main factors, which determine bandwidth of the diffusion zone in the case of pulse irradiation, are pulse duration and power density of the plasma jet.

The coating before melting by plasma jet has the seeable boundary with the substrate (Figure 3a). You can see on Figure 3a the particles of coatings' powder. There is no penetration of substrate elements in the coating stated by the EDS methods (Table 2).

After pulse plasma treatment (melting), these coatings have a good adhesion to substrate (Figure 3b). The homogeneous microstructure with average grain diameter 5 μm is formed. The increase of Fe mass fraction in the coatings is established by EDS (Table 2). The distribution of Fe in coating is inhomogeneous. The content of Fe decreases from surface to substrate (Table 2), but even at the depth on the order of 30 μm from the coating surface, it is by an order of magnitude greater than Fe head grade in the coating.

TABLE 1
Elementary Composition (in wt.%) through the Thickness of the Coating Made of Ni–Cr after Melting, and Steel Substrate at the Points, Marked In

Spectrum	Si	Cr	Mn	Fe	Ni	Total	Comment
Spectrum 1	2.76	11.56		44.75	40.93	100.00	Coating surface
Spectrum 2	1.99	7.97		59.96	30.09	100.00	Coating
Spectrum 3	1.60	6.06	0.42	68.16	23.75	100.00	Coating, transition layer
Spectrum 4		0.31	0.55	84.02	15.12	100.00	Substrate, transition layer
Spectrum 5			0.63	99.37		100.00	Substrate
Spectrum 6			0.51	99.49		100.00	Substrate

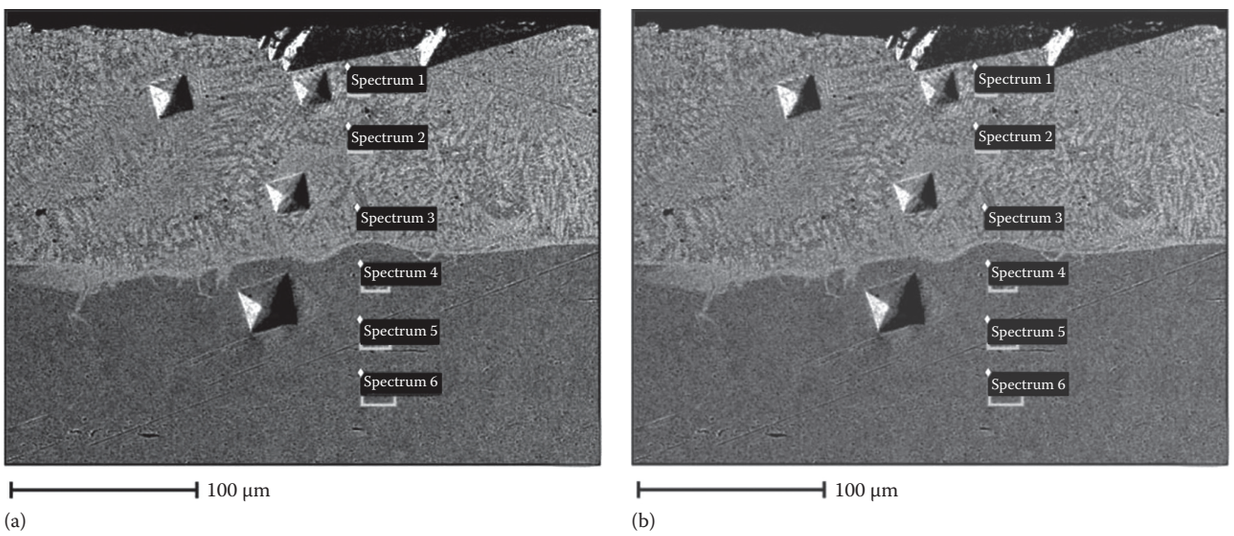

FIGURE 3 (a) SEM images of cross section plasma detonation powder coating Ni–Cr. The areas where the element analysis was made are marked. Shot in the mode of secondary electrons. Catch sight of microhardness tester indenter imprints in the coating is at the bottom of the picture. (b) Image of the coatings after pulse plasma treatment (melting).

TABLE 2
Results of Element Analysis (wt.%) of Plasma Detonation Powder Coating Ni–Cr

Spectrum	Si	Cr	Mn	Fe	Ni	Note
5			0.36	99.64		Substrate
4			0.35	99.65		Substrate, intermediate layer
6	3.42	10.66		4.27	81.64	Coating

AQ4

TABLE 3
Results of Element Analysis (wt.%) of Plasma Detonation Powder Coating Ni–Cr after Pulse Plasma Treatment (Melting)

Spectrum	Si	Cr	Mn	Fe	Ni	Note
1	2.76	11.56		44.75	40.93	Surface of coating
2	1.99	7.97		59.96	30.09	Coating
3	1.60	6.06	0.42	68.16	23.75	Substrate, intermediate layer
4		0.31	0.55	99.14		Substrate
5			0.63	99.37		Substrate
6			0.51	99.49		Substrate

Using RBS method, we detected high concentration of Mo through the thickness of the coating Ni–Cr up to 12 μm (near 20 at.%) (Figure 4).

Due to plasma jet–induced heating, the coatings became structurally homogeneous, fine-grained structure appears with an average grain size 2 μm (Figure 5). Volume fractions

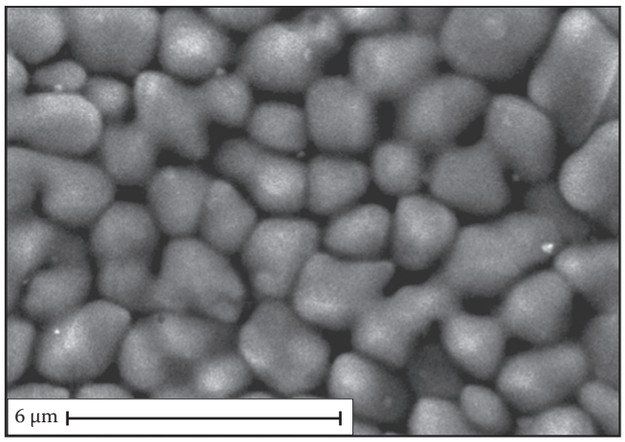

FIGURE 5 Microstructure of the coating made of Ni–Cr after melting.

of solid solution and intermetallic phases increase due to diffusion speedup by pulse plasma and noninterruptible pulse plasma jet.

Investigations of Co–Cr coatings using SEM shows (Figure 6) that discrete border is formed between coating and substrate under mentioned deposition regimes. As a result of plasma flux impulse both with melted powder, part of surface layer become deformed (both with powder particles), but at the same time, powder particles implants in melted surface (or in partly heated substrate layer).

Transition layer zone (so-called thermal influence zone) and thermomechanical influence zone (so-called cold hardening) are observed behind the interface border approximately at the coating depth.

From Figure 7b and c, we can see that coating, which was deposited in two passes, has several differences in structure

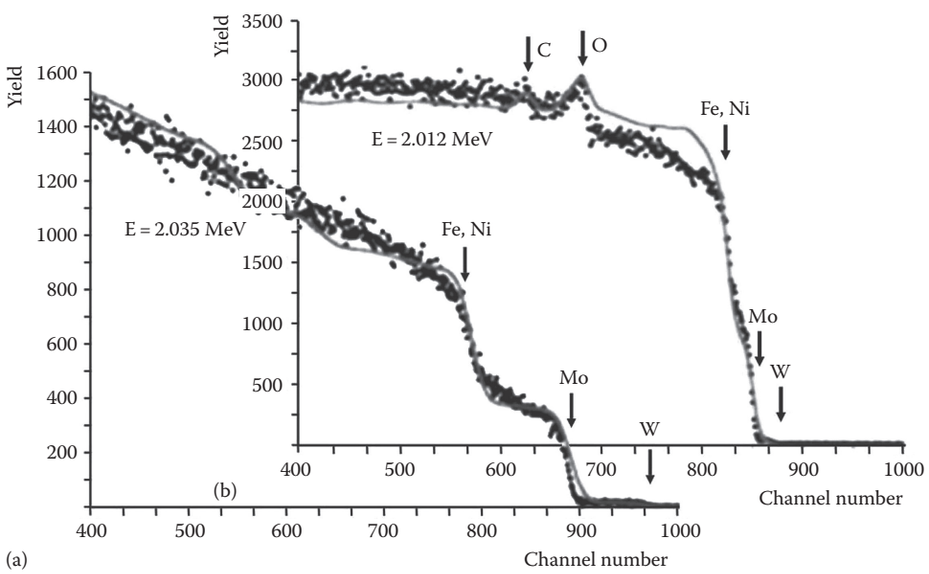

FIGURE 4 Energy spectrums of Rutherford backscattering of ions He^{4}_{+2} with energy E = 2.035 MeV (a) and protons with energy E = 2.012 MeV (b), from the surface layer of the coating made of Ni–Cr. AQ5

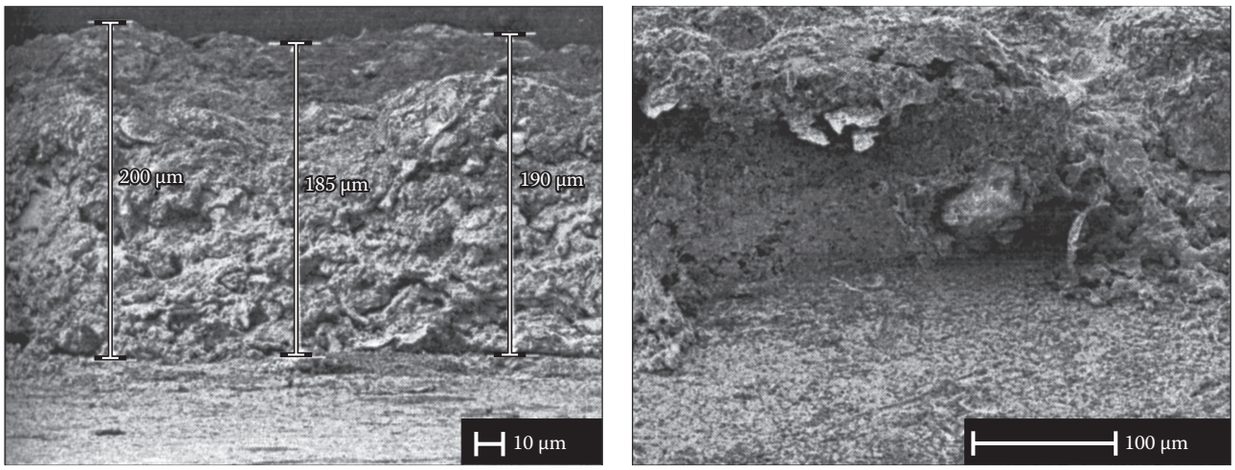

(a) (b)

FIGURE 6 (a) Microstructure of Co–Cr coating, which was deposited by two passes. (b) Microstructure of the interface layer between substrate and coating.

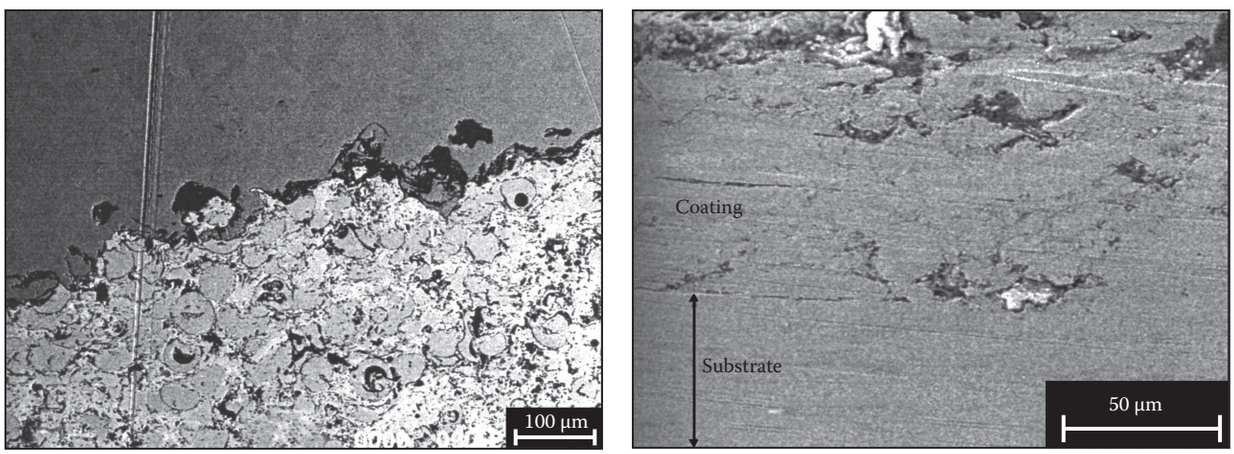

(a) (b)

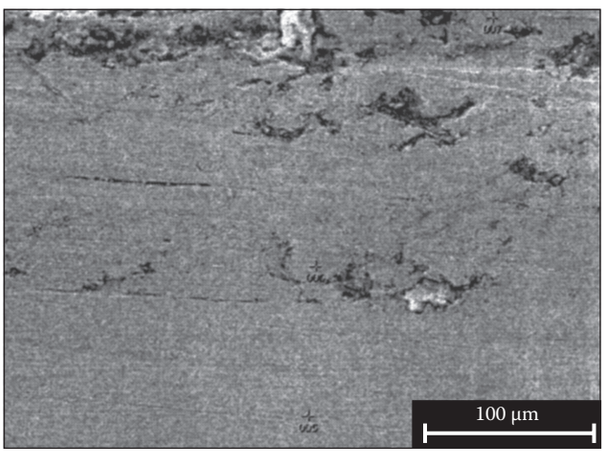

(c)

FIGURE 7 (a) View of the interface between substrate and Co–Cr coating (angle cross section, coating is in the bottom). (b and c) Image of the cross section of the sample with Co–Cr coating (in the electron backscattering regime).

of layers. Two layers of the coating and a border between coating and substrate are observed. Through-the-thickness elementary composition analysis (in at.%) for Co–Cr coating is presented on Figure 7 at the indicated points.

As we can see from Figure 8c and e, Fe particles implants from substrate into coating on the specified area, its amount considerably changes, and depends on the initial coating composition. Cr content decreases noticeably with the depth, but Co content is staying put.

We can see noticeable border between substrate and coating, made of Co–Cr (Figure 7b). If we will consider, that during deposition of the second layer of the Co–Cr coating, part of the plasma flux energy is spending up on melting of the new deposited powder particles, then full heating (melting) of the coating layer don't occur. Pulsed influence of the plasma jet stimulates diffusion processes, but that influence is nonuniform, as well as sample heating is nonuniform on the depth.

Distribution of the Co–Cr coating elements (with steel substrate, based on Fe) are presented on the Figure 8a–e. It is clearly seen from this Figure, that substrate parts penetrates into coating on the length of 50 μm and on the depth of 22–25 μm. Penetration of substrate parts is connected with thermoelastic stresses and mechanical movements of the rigid fragments of the coating into melted region under plasma flux and fritted (melted) powder particles influence in the time of repeated passing of the jet with powder. These results also correlate with x-ray structure analysis of the coating and substrate on different depth and with microhardness measurements, which will be provided in later text.

According to performed studies of morphological features of the surfaces after their treatment by HVPJ, they melted, which resulted to essential smoothing of the relief and decreased roughness dimensions in the coating surface. However, some particles (depending on their initial dimensions), being treated by HVPJ for the second time, did not melt. They only sweated together with other nonuniformities. SEM analysis performed in some regions of the coating demonstrated that the same structure as in the case of concentrated energy flow treatment was formed in the surface.[2–7,10–18]

Coating surface morphology studies demonstrated that some changes took place in the coating matrix under selected regimes of surface thermal modification. The obtained photos show that the HVPJ treatment was accompanied by through melting of the surface since an amount of nonfully melted powder particles decreased essentially in the coating matrix. Traces of some powder particles remained in the photos, but they were significantly lower in diameter (Figure 9a), and the coating itself had higher degree of alloying. Surface melting by pulsed plasma flows provided also changed element composition of near-surface coating layers.

Coating surface morphology studies demonstrated that some changes took place in the coating matrix under selected regimes of surface thermal modification. The obtained photos show that the HVPJ treatment was accompanied by through melting of the surface since an amount of nonfully melted powder particles decreased essentially in the coating matrix. Traces of some powder particles remained in the photos, but they were significantly lower in diameter (Figure 9a), and the coating itself had higher degree of alloying. Surface melting by pulsed plasma flows provided also changed element composition of near-surface coating layers. AQ6

But in the process of melting, an amount and dimensions of these pores essentially decreased, and those that remained were filled-in by atoms of the eroding electrode. Figure 9b demonstrates the structure of near-surface regions of the resulting coating more clearly. Studies of the surface element composition by microanalysis demonstrated that these light aggregates by 95% are composed of molybdenum atoms. Integral spectra of the coating surface element composition after melting demonstrated high-intensity chromium, iron, and cobalt peaks (Figure 9b). Distribution of basic coating elements over depth at points, which are marked in (Figure 10) are summarized in Table 4. According to obtained result of analyses distribution of the coating composing elements practically does not change from point to point. We assume that presence of molybdenum atoms in powder coatings was due to its presence in the plasmatron gas atmosphere and the result of deposition process, since distribution of molybdenum atoms over the coating depth and width shows uniform character. However, physical and mechanical surface properties are determined not only by its morphology and elements composition.

Figure 11 shows the energy spectra of Rutherford proton backscattering obtained for the sample with Co–Cr coating, whose surface layer was melted by a plasma jet to the depth not lesser than 40 μm. Table 5 summarizes the coating composition over its depth, which was obtained from the energy spectra of RBS analysis using a standard program. As one can see from the Figure 12 and Table 5, after melting in the powder coating on Co–Cr base, one can find not only 54.72 to 74.16 at.% of Co, 14.41 to 19.67 at.% of Cr but also 0.93 to 1.26 at.% of W. In addition, in this coating, we found about 5 at.% of Ni, which concentration grows a little in comparison with initial state. In the sample surface (or in the near-surface region), we found an oxygen, the concentration of which reached 25 at.% up to 0.3 μm depth.

Using Mössbauer spectroscopy, we established that in the Ni–Cr coating matrix in the region, contacting with the substrate, there are the finest particles of α-Fe. It confirms acceleration of diffusion processes by plasma jet.

Fine-grained homogeneous coating structure (with volume fraction of γ-solid solution up to 85%, intermetallic phases are created after its decomposition) is formed due to irradiation.

For a detailed analysis of the coating thin structure, we have used such methods as TEM and XRD on different distance from the surface (layer-wise research). Also, we measured microhardness and sizes of structural units of all the materials of the coatings and substrates on the different distance from surface using beveled samples.

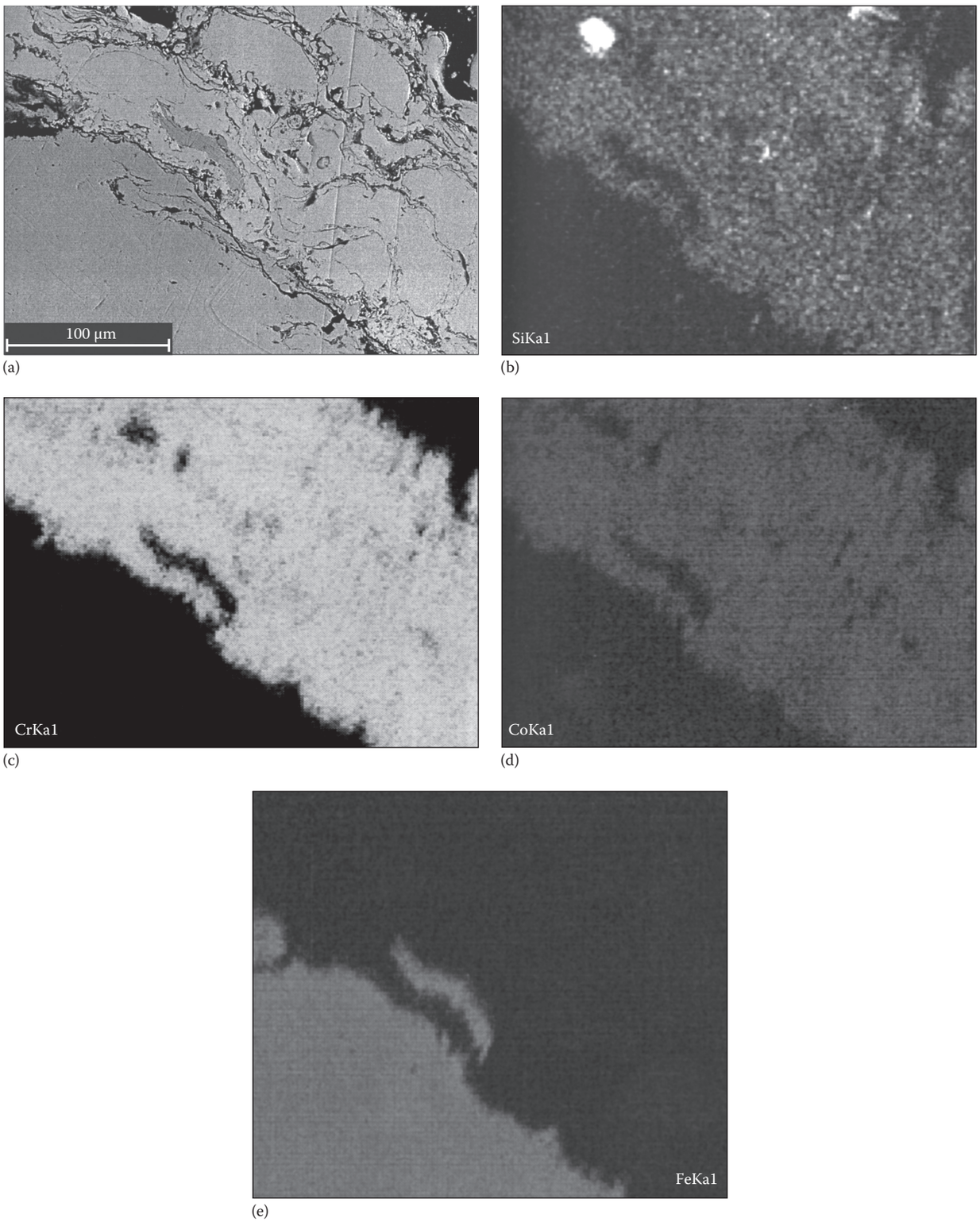

FIGURE 8 SEM image of the contact zone between Co–Cr coating and steel substrate. (a) Elementary distribution map for substrate; (b–e) elementary distribution maps for Co–Cr coating, based on the steel substrate (with Fe base).

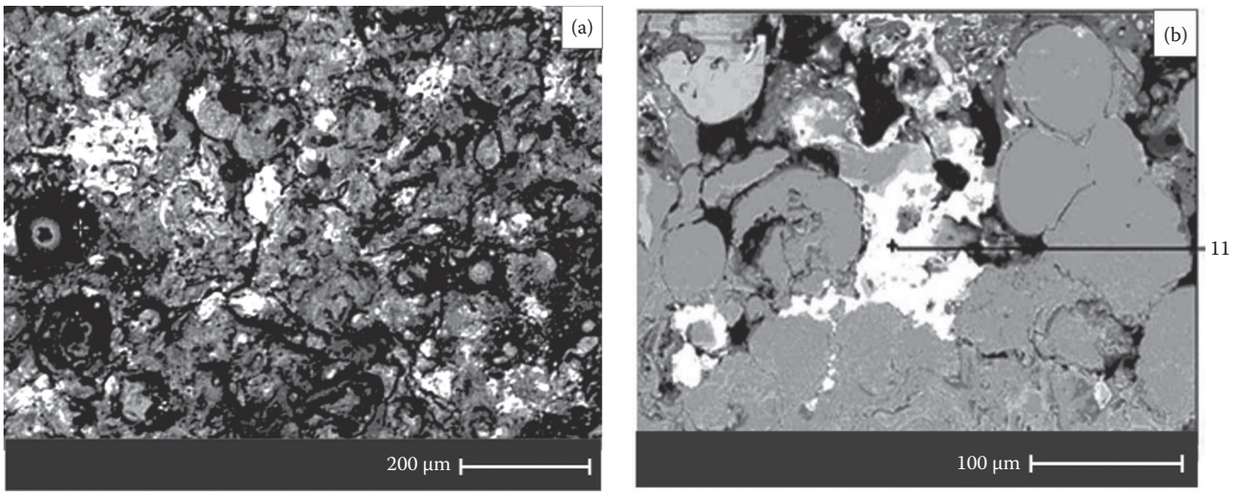

FIGURE 9 Effect of high-velocity pulsed plasma flows on the structure and element composition of Co–Cr powder coating surfaces: (a) a general view of the surface obtained using secondary electrons; (b) integral chemical composition of the surface region presented in Figure 9a.

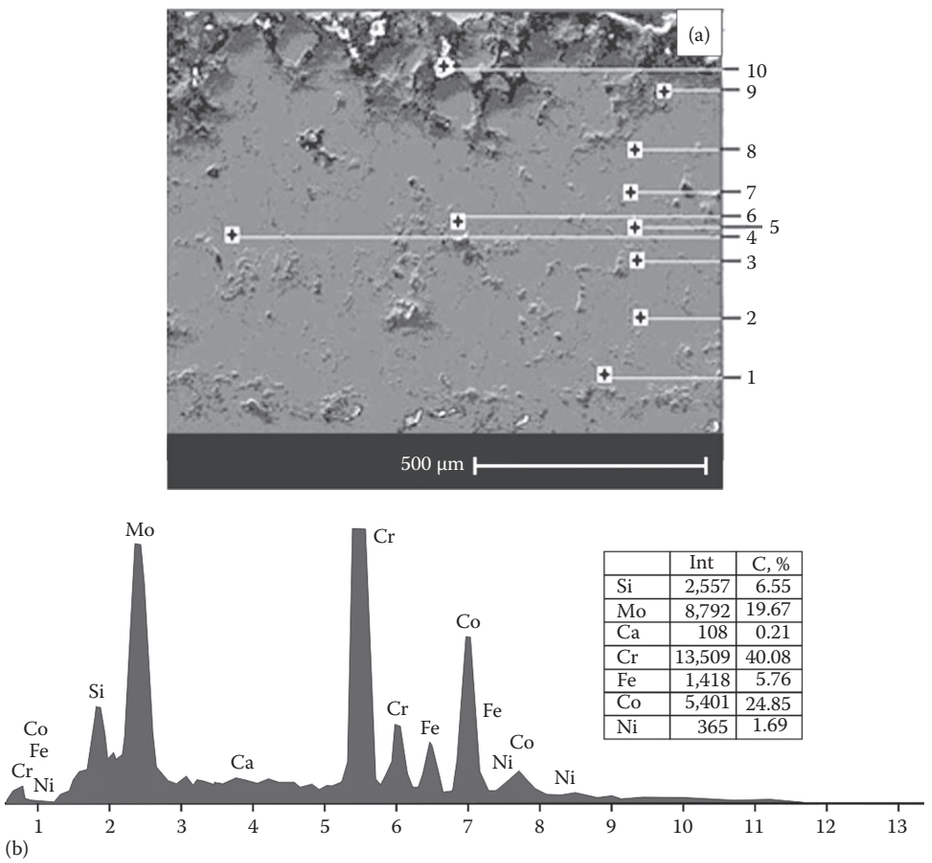

	Int	C, %
Si	2,557	6.55
Mo	8,792	19.67
Ca	108	0.21
Cr	13,509	40.08
Fe	1,418	5.76
Co	5,401	24.85
Ni	365	1.69

FIGURE 10 Results of studies for distribution of coating element composition over depth after HVPJ treatment (crosses mark the points of local element analysis): (a) photos for some region of the powder coating cross section; (b) the structure of powder coating near-surface regions after melting (in the electron backscattering regime).

TABLE 4
Distribution of Elements Content over Depth of Powder Coatings after HVPJ Modification

Point N	C at.%	Si at.%	Mo at.%	Cr at.%	Fe at.%	Co at.%	Ni at.%	W at.%	Mn at.%
1	0.45	1.34	1.00	31.56	1.86	57.35	2.71	2.73	—
2	0.53	0.33	2.64	17.56	66.19	1.08	10.69	—	—
3	0.51	1.33	1.02	30.09	1.74	58.7	3.06	2.56	—
4	—	2.26	1.38	32.32	1.52	57.42	3.48	—	0.61
5	—	2.24	1.21	30.51	1.92	55.87	7.26	—	0.48
6	—	2.51	1.39	31.86	1.59	57.41	3.56	—	0.69
7	0.48	1.13	1.08	30.07	2.82	57.86	3.05	2.5	—
8	0.78	1.12	0.99	29.61	3.17	57.86	3.01	2.45	—
9	0.62	0.98	0.95	30.45	2.45	58.27	2.7	2.55	—
10	—	—	94.33	—	1.34	3.33	—	—	—
11	—	—	97.99	0.30	—	0.71	—	—	—

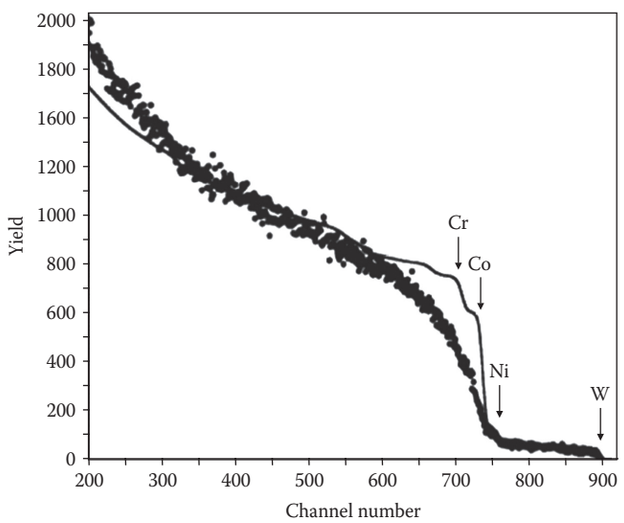

FIGURE 11 RBS energy spectrum obtained using proton beam Ep = 2.04 MeV for stainless steel with coating of Co–Cr after plasma jet melt (θ = 170°, φ = 60).

TABLE 5
Distribution of Elements Content over Depth of Powder Coatings after HVPJ Modification

	Element Concentrations, at.%				
Depth, nm	W	Ni	Co	Cr	O
70.4	0.93	4.90	54.72	14.41	25.04
139.2	0.90	4.90	58.72	14.02	21.46
307.6	0.88	4.90	64.63	13.83	15.76
4902.2	1.26	4.91	74.16	19.67	0.0
15240.1	1.26	4.91	74.16	19.67	0.0

When the coating porosity is low, their hardness will be dependent on the surface phase composition. Using x-ray analysis, we found that the powder that was used for deposition was composed of a solid solution α- and β-Co.

Forming of the γ-solid solution with face-centered cubic (FCC) lattice, based on the basic compound of the coating (Co or Ni accordingly), is characteristic, in general, for the main coating's thickness. Intermetallic phases are separated: $Co_{0.8}Cr_{0.2}$ (hexagonal, P 63/mmc, a = 2.52 Å; c = 4.062 Å) or $CrNi_3$ (FCC lattice, Fm-3m, a = 3.552 Å) or Fe_7Ni_3 (BCC lattice, Im-3m, a = 2.861Å) or $FeNi_3$ (primitive cubic lattice, P 213, a = 3.5450 Å).

Before coating deposition using plasma detonation technique, we did not observe intermetallic phases in coating powders. Generally, they consist of solid solution based on Ni or Co with FCC lattice. In powder Co–Cr, we have also observed solid solution based on Co with FCCP lattice. At the same time, there were different impurities (about 10–25 vol.%); see Figure 13.

Existence of Mo on the surface of the coatings made of Ni–Cr и Co–Cr, which were irradiated by plasma flux under pulse regime, is detected by SEM data with microanalysis, and it depends on its ingression into material from Mo electrode (Figure 14). Additional alloying of the coatings surface by Mo takes place due to pulse plasma melting. Before coating deposition using plasma detonation technique, we did not observe intermetallic phases in coating's powders. Generally, they consist of solid solution based on Ni or Co with FCC lattice. In powder Co–Cr, we have also observed solid solution based on Co with FCCP lattice. At the same time, there were different impurities (about 10–25 vol.%), see Figure 15.

From experimental layer-wise analysis, it is obvious that the phase-structure composition differs along the coating thickness. During deposition using plasma detonation technique, melting and fragmentation of the powder particles occur after hitting the substrate, impurity phases dissolve, and γ-solution is formed from the flux and decayed. Lattice parameter of the γ-solid solution in such coatings decreases through the thickness, and the diffusion zone is formed with the enhanced microhardness in comparison with a substrate.

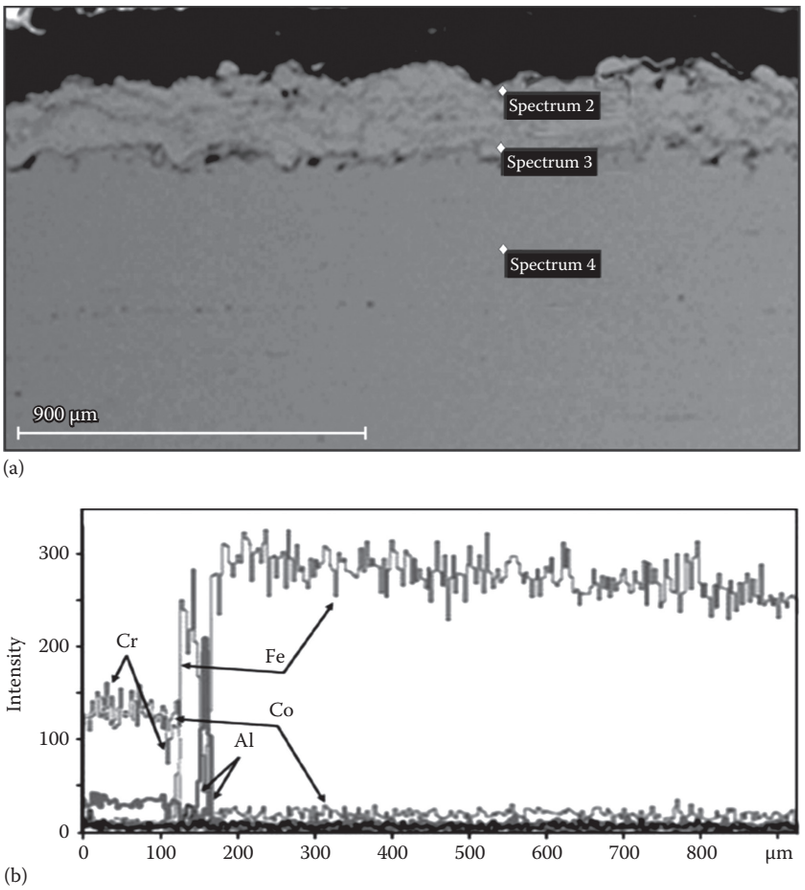

FIGURE 12 Image of the cross section of the sample with Co–Cr coating, after plasma jet treatment, which was obtained in the electron backscattering regime (a), and element distribution on the thickness of the coating and substrate (b).

There are a lot of phases, based on Fe, in the contact with a substrate layer. The substrate is α-Fe with BCC lattice with parameter a = 2.8662 Å.

On the surface of the coatings, we can observe the thin layer of the solid solution with amorphous structure (thickness is not greater than 5 µm) with oxides and carbides. Thickness and composition of the thin surface layer were detected using sliding x-ray beam and electron-chemical spectral analysis with etching of the upper layer using Ar ions.

Obtained by TEM, data confirm the formation of the superfine grained (nano) structures in the coating Ni–Cr and Co–Cr. Using TEM methods, we found that Co–Cr coatings were formed by nanograins of different crystallographic orientation (Figure 16a), and intermetallic phases morphology were lamellar (Figure 16b). On XRD pattern and on γ-phase annular micro–electron diffraction pattern, we observe textures with type <111> zone axis (Figure 16a). In the coating layer contacting with the substrate, we observe deformation bands (Figure 16b).

In the surface layer of the Co–Cr coating, there are enough parts with amorphous structure (Figure 16c and d), we can see halo scattering on the micro–electron diffraction pattern of this region (Figure 16d). This matches with XRD data, which show the existence of the x-ray-amorphous layer on the surface.[21,23,24,42] Near the coating, there are regions, where crystallographic planes are located in the ordered arrangement along one direction (Figure 17a). Length of such regions is near 15 µm (Figure 17a and b), local ordering is noticed within one subgrain; in other words, it is microscopic formation, which determines structure of the microscopic regions of the coating, texture is also formed. At the same time, there are regions with nanograins crystallographic disordering (Figure 49.17c). As opposed to Ni–Cr coatings, textured regions dominate in the Co–Cr coatings.

Thereby, using high-resolution TEM methods, we obtained that solid solution in the Co–Cr coatings is formed by nanograins of different crystallographic orientation and intermetallic phase's separation morphology is lamellar. On the annular micro–electron diffraction patterns of the coating matrix (electron beam alignment is normal to the coating surface), we can see texture with zone axis of the type <111>, and it corresponds to fibrous texture of the grains growth along heat flow in the coating.

Due to chaotic crystallites location in regard to each other in fine-dispersed units on the annular microdiffraction pattern, we can see all plane circular reflections (220), (422), (440), which belong to texture with the axis of the type <333> and have greater intensity.[22,23]

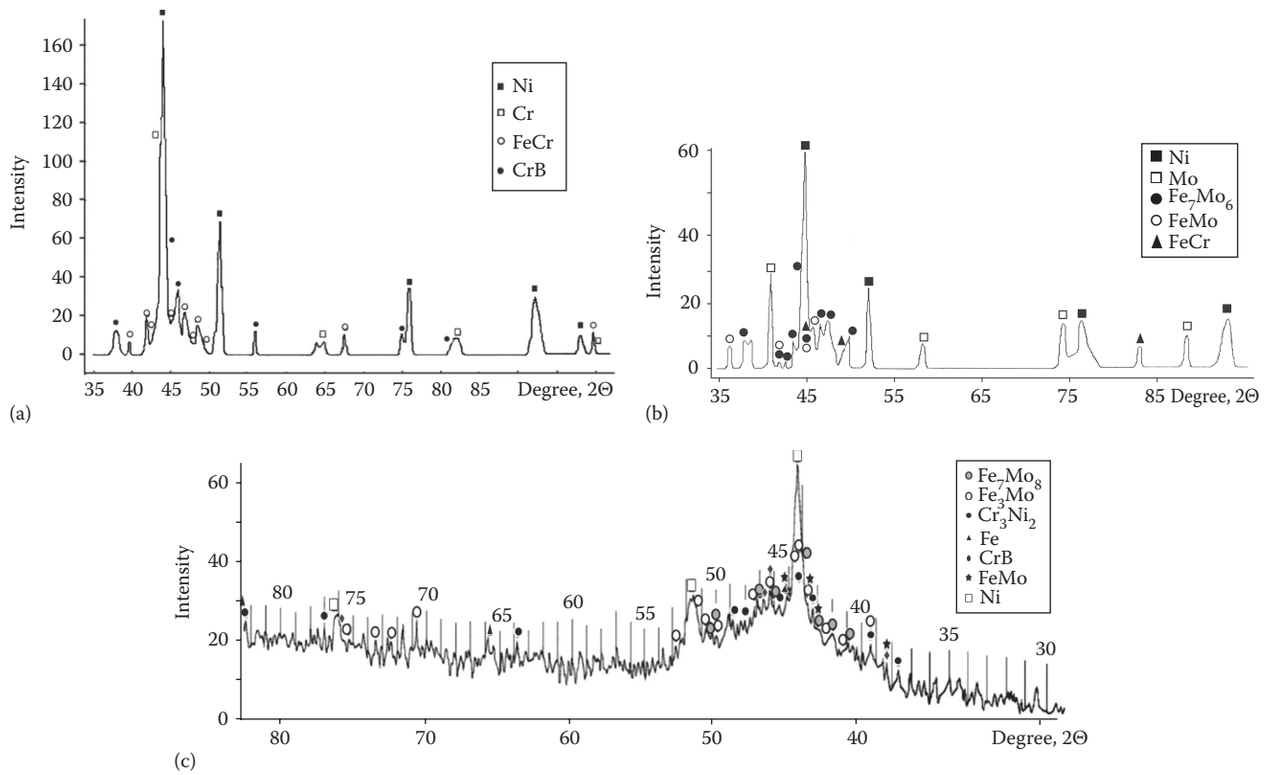

FIGURE 13 Diffraction patterns (XRD) for steel samples with Ni–Cr coatings of about 120 μm thickness, which were deposited using high-velocity plasma jet: (a) as deposited; (b) after subsequent treatment by plasma jet of about 5×10^6 W/cm^2 power density; (c) diffraction patterns (XRD) for Ni–Cr coating of the thickness 120 μm, which were deposited using HVPJ and after subsequent treatment by plasma jet with three passes (5×10^6 W/cm^2).

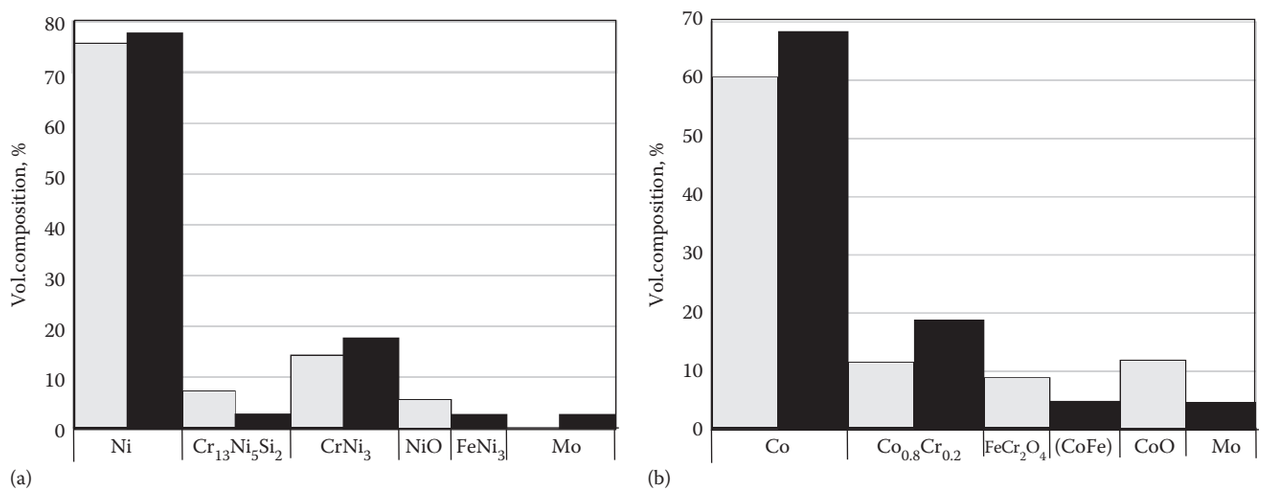

FIGURE 14 Comparison of two-phase composition of the coatings made of Ni–Cr and Co–Cr before (light-colored columns) and after (dark-colored columns) melting. (From Gorelik, S.S. et al., *X-Ray and Electron Optic Analysis*, MISIS, Moscow, Russia, 1994; Oliver, W.C. and Pharr, G.M., *J. Matter. Res*., 7(6), 1564, 1992; Ageev, N.V. and Petrov, L.A. Ed., *State Diagrams of Metallic Systems*, Moscow, Russia, 1985, pp. 60–62.)

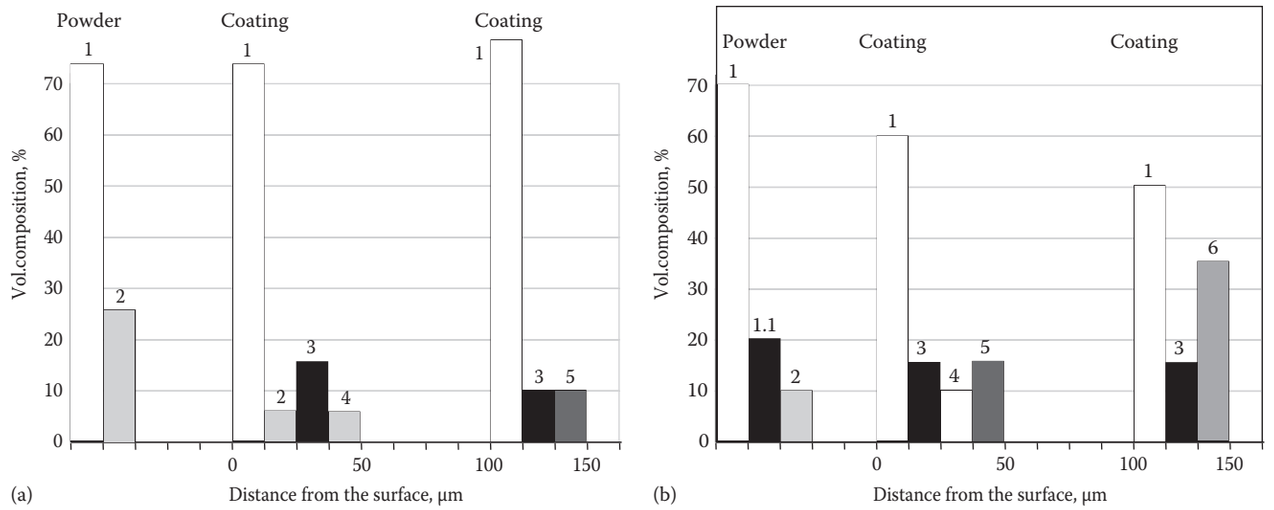

FIGURE 15 Differences in phase composition of powders and coatings and in composition of the coating through the thickness from surface, which were obtained using XRD analysis: 1—Ni, 2—$Cr_{13}Ni_5Si_2$, 3—$CrNi_3$, 4—$NiFe_2O_4$, 5—Fe_7Ni_3 (a); 1—Co (FCC), 1.1 – Co (FCCP), 2—Co–Cr_2O_4, 3—$Co_{0.8}Cr_{0.2}$, 4—$FeCr_2O_4$, 5—CoO, 6—(CoFe) (b). (From Gorelik, S.S. et al., *X-Ray and Electron Optic Analysis*, MISIS, Moscow, Russia, 1994; Oliver, W.C. and Pharr, G.M., *J. Matter. Res*., 7(6), 1564, 1992; Ageev, N.V. and Petrov, L.A. Ed., *State Diagrams of Metallic Systems*, Moscow, Russia, 1985, pp. 60–62.)

Using TEM methods for thin foils, we analyzed structure-phase state of the coating: near surface, inside it (approximately in the middle of the coating), and close to the substrate region.

AQ7 Coatings, based on Ni–Cr, are polycrystalline solid solutions, and based on Ni, with FCC lattice, it consists of nanograins with different crystallographic orientation (Figure 18a and b). According to XRD data, solid solution lattice parameter a = 3.5250 Å. According to micro–electron diffraction pattern (Figure 18d), this parameter equals to 3.5 Å. The size of particular nanograins is 2–3 nm, grain borders are unnoticeable, nanograins are azimuthally disoriented on the angles more than 10°, and micro–electron diffraction pattern of the coating is annular (Figure 18d). We should note that the structure of the coating basis is similar to the crystallographic disoriented nanograins structure (Figure 18a). Figure 18b demonstrates this statement.

Solid solution decay regions are lamellas (length from 30 to 50 nm) of the $CrNi_3$ intermetallic phase with FCC lattice

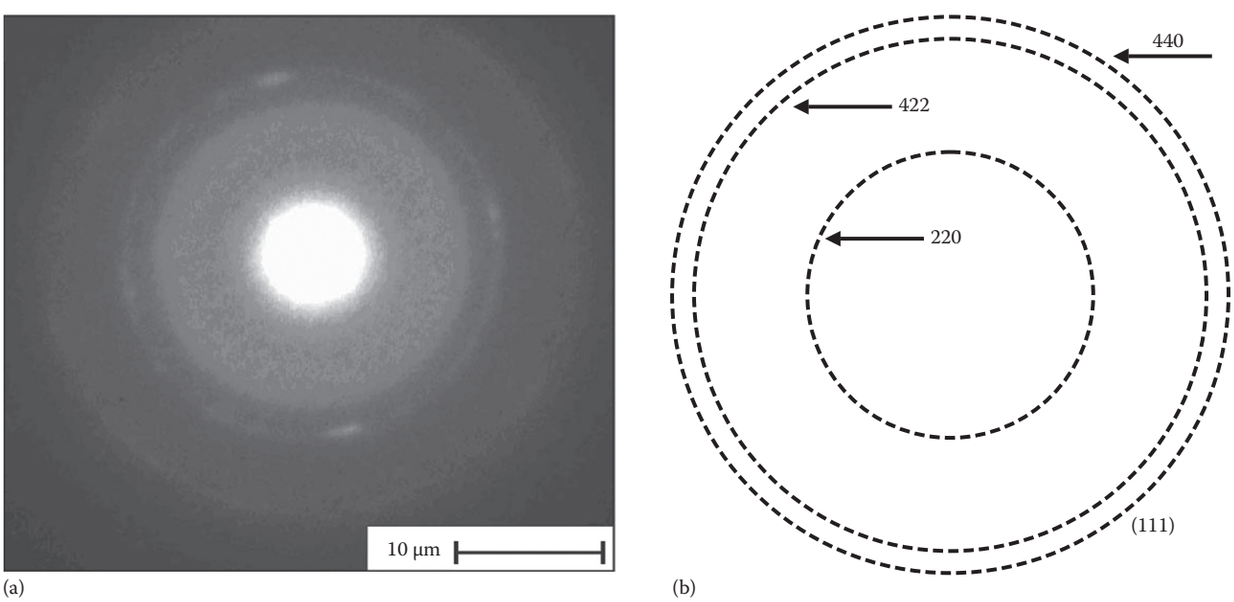

FIGURE 16 Micro–electron diffraction pattern of the Co–Cr coating (a) and scheme, which describes the structure creation with the zone axis of the type <111> (b); (*Continued*)

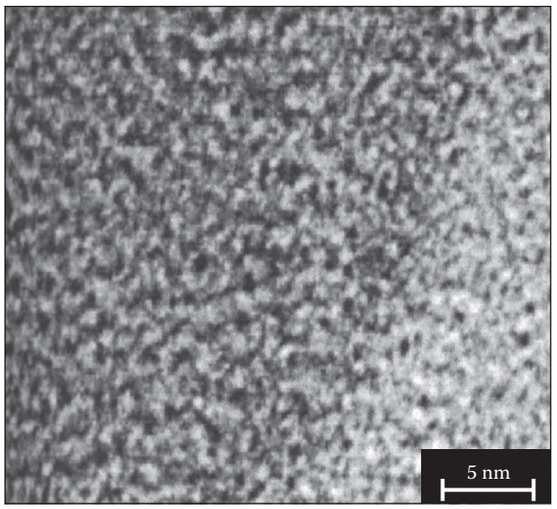

(c)

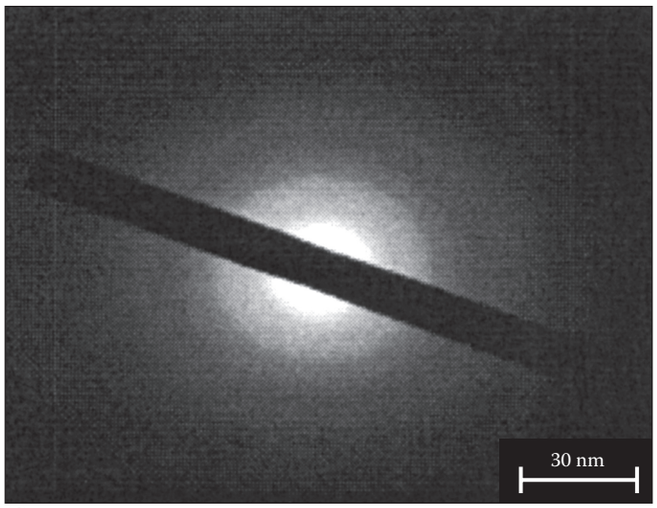

(d)

FIGURE 16 (*Continued*) (c and d)—TEM image of the microstructure of the surface layer of the Co–Cr coating—part with amorphous structure (c), and its micro–electron diffraction pattern (d).

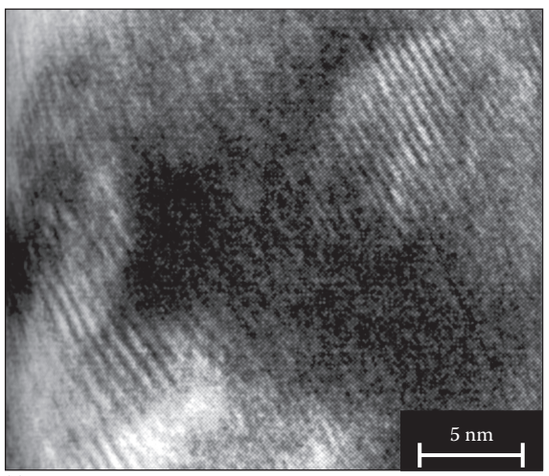

(a)

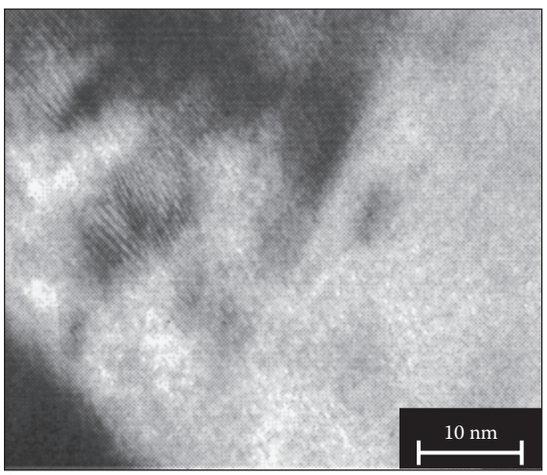

(b)

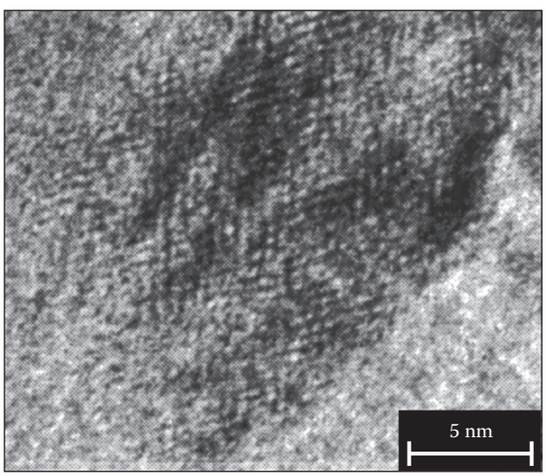

(c)

FIGURE 17 TEM image of the regions of the Co–Cr coating: (a) with disoriented atomic planes; (b) parts with texture, and (c) part with disoriented planes.

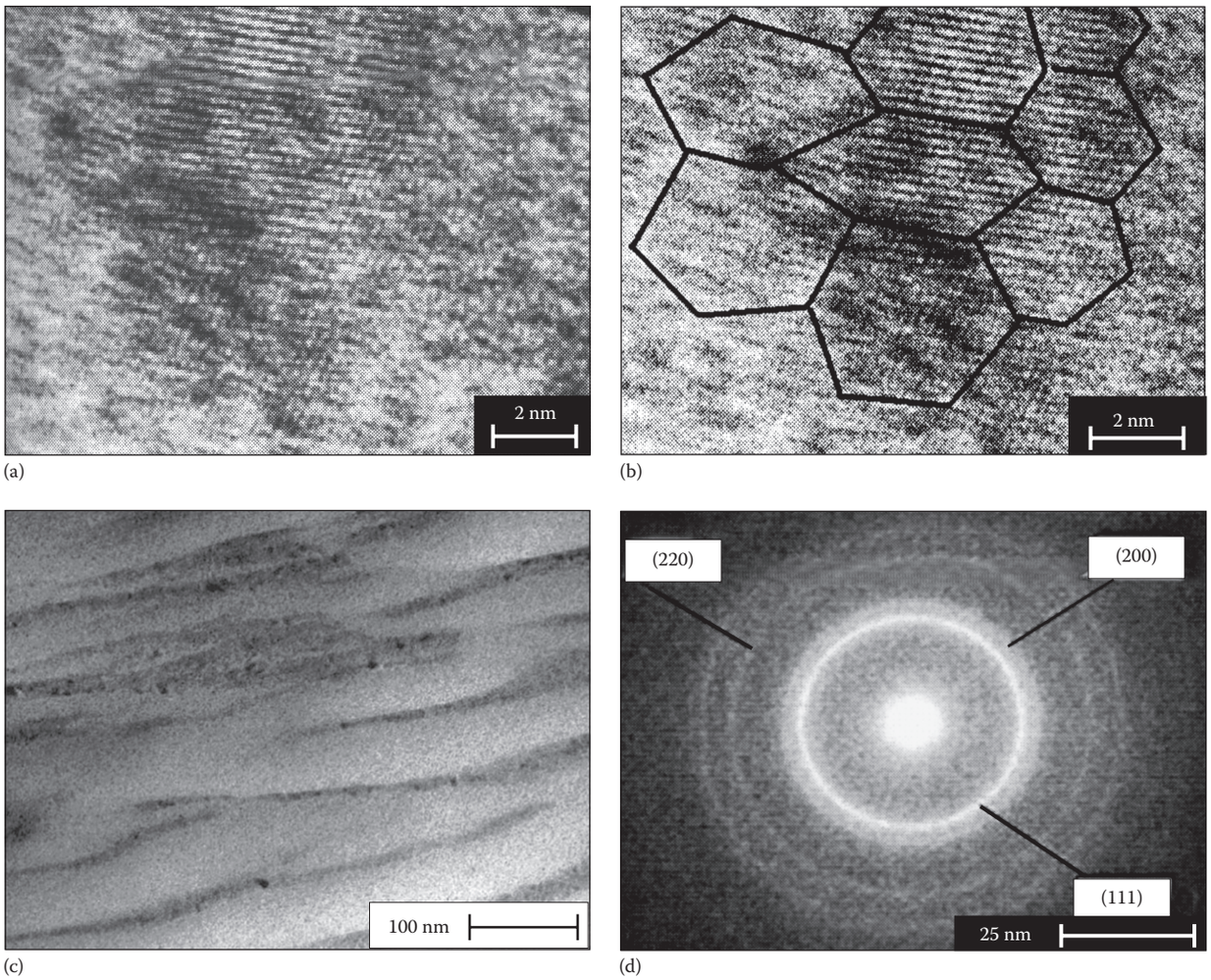

FIGURE 18 TEM images and microdiffraction photos of the nanograins with different crystallographic orientation in the coating made of Ni–Cr (a); grain borders on TEM image (b); deformation bands in the layer of the Ni–Cr coating, which contacts with substrate (c); micro–electron diffraction pattern of the matrix with plane indexes (d).

in the coating, made of Ni–Cr (Figure 19a), and lamellas of the $Co_{0.8}Cr_{0.2}$ intermetallic phase with hexagonal lattice in the coating, made of Co–Cr (Figure 19c). Lattice parameters of such phases and solid solutions, obtained after micro–electron diffraction pattern interpretation (Figures 19b and 19d) practically coincide with the values, which were obtained using XRD. Every indicated reflex of the intermetallic phase on micro–electron diffraction pattern was checked using dark field method.

Volume fraction of the intermetallic phases differs through the coating thickness; it was determined using XRD and TEM (Figure 19).

Volume fraction of strengthening intermetallic phases is higher besides the coating before irradiation (Figure 20); diffusion zone bandwidth increases by 50 μm between the coating and substrate.

Figure 20 shows the scheme of the plasma detonation powder coating structure. The first zone is the coating surface, characterized by the solid solution amorphization and presence of the oxides. The second zone has the structure with the bigger prolonged grains. These grains with the light boundary contrast (with 5 μm diameter cross sections) can be observed on the images of the coating foil, which were explored using the SEM methods (Figure 20b).

The thickness of the second zone actually coincides with the coating thickness. Inside the prolonged grains, we can observe the structure, constructed of misaligned nanograins and areas of the ordered solid solution with the size of 50 nm. Inside these areas, solid solution decay occurs with the intermetallic phase lamellas releasing (Figure 20c).

In general, the coating structure is nanocrystal over the thickness with the nanosize intermetallic lamellas volume fraction of 20%–30%. The reason for occurrence of the misaligned nanograins is the high microdefect structure, specified by deformation after applied plasma jet shock and high-temperature gradient in the coating. The substructure, made of nanograins of different crystallographic orientation, is created in the coating for mechanical stresses relaxation.

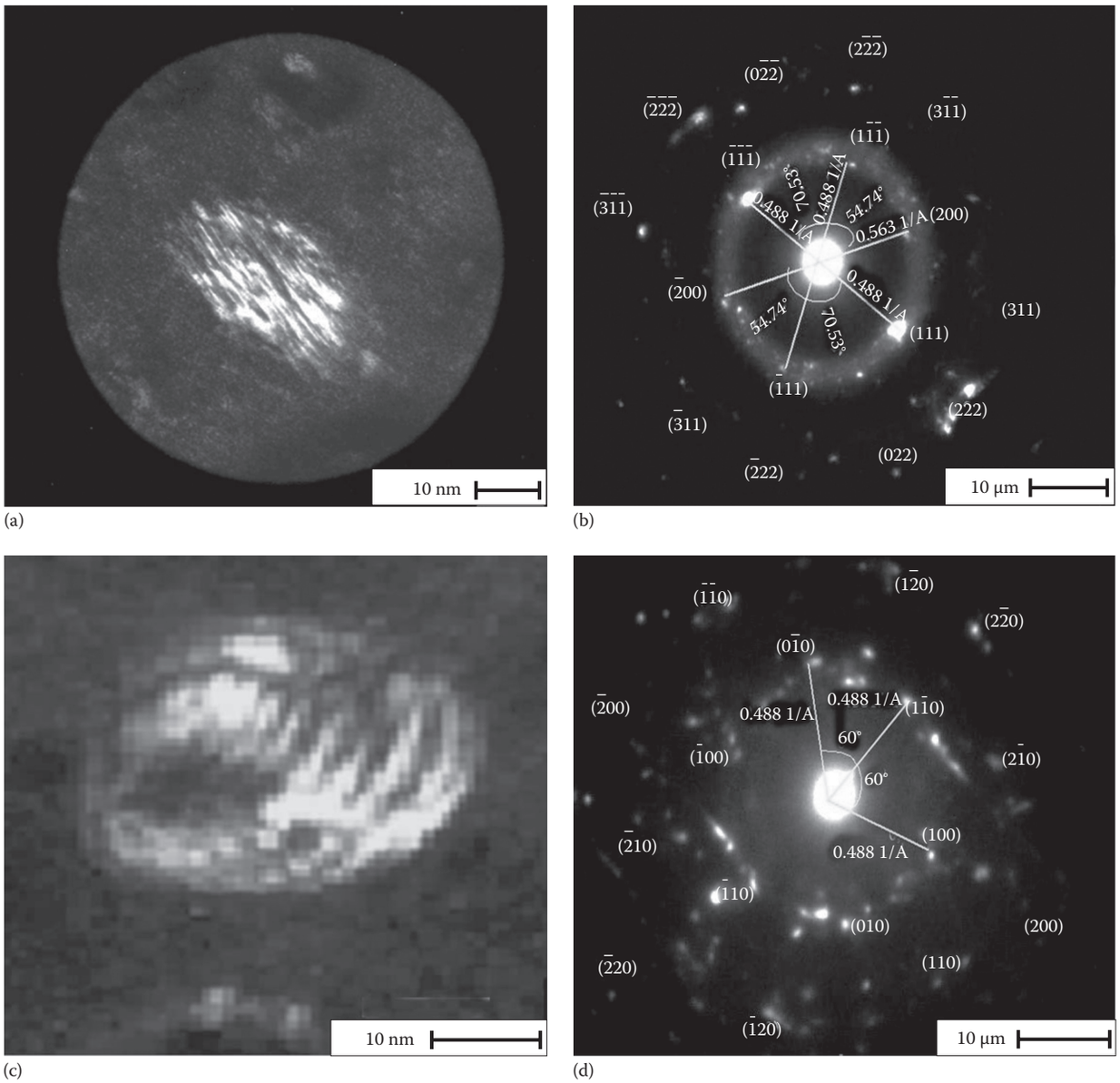

FIGURE 19 TEM image and microdiffraction image of the Ni–Cr coating: $CrNi_3$ particles, dark field, being shot in reflection (111) (a); micro–electron diffraction pattern of the $CrNi_3$ particles, zone axis [1 $\bar{1}$ 1] (b); microdiffraction image of the Co–Cr coating: $Co_{0.8}C_{0.2}$ particles, dark field, being shot in reflection [1 $\bar{1}$ 0] (c); micro–electron diffraction pattern of the $Co_{0.8}C_{0.2}$ particles, zone axis [001] (d).

The substructure is similar to the fragmentary structure with fragments–grains misalignment, analogous to the polygonization of crystals. The formed nanostructures are stable under room temperature, they are observed in the coating foils, treated several months and even years ago, their strength properties remains the same. The width of such band is 100–150 μm.

The structural phase composition of the mentioned area is interchanging of the solid solution, based on the coating material, solid solution, and iron with FCC-packed lattice structure. We assumed the diffusion of the main structural components of the coating (Ni or Co, respectively) to the substrate and Fe components from the substrate to the coating. We estimated the diffused zone width to be 100 μm in the average: 50 μm, in the coating and 50 μm, in the substrate.

Inhomogeneous microhardness distribution along the coating thickness is observed. Maximal values of microhardness correspond to the parts of the coating with the lowest volume fraction of aforementioned intermetallic phases (Figure 21). At the same time, microhardness curves point at the existence of the transitional zone with the enhanced microhardness between the coating and substrate. According to XRD analysis data, we can call it a diffusion zone (Figure 21). Its width is about 100 μm.

On two other figures, we present results of measuring of microhardness along the thickness of the Ni–Cr coatings

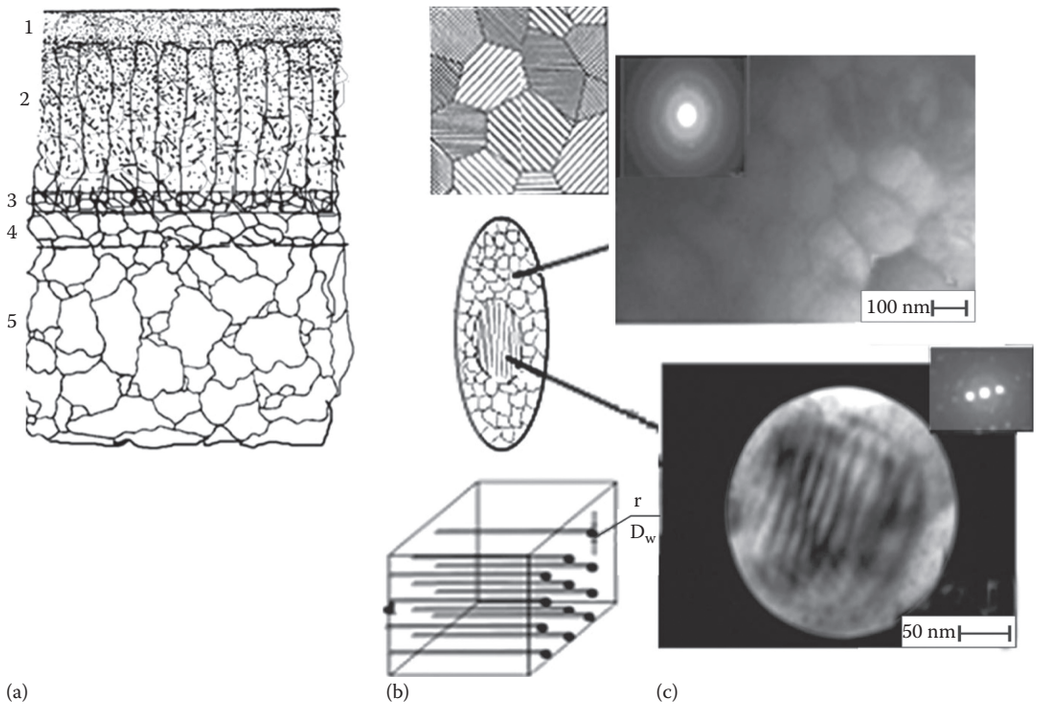

FIGURE 20 (a and b) Schematic picture of the structure of the coating, treated by the plasma detonation method on the steel substrate: (1) amorphous layer with oxides and carbides; (2) textured coating matrix (solid solution, based on the main component of the coating, intermetallic phases are selected) and unfused powder particles; (3) transition layer from coating to substrate, with deformation areas in the coating, with grinded powder particles; (4) transition layer with the substrate granular grains; (5) substrate. (c) Shows the texture of the coating grain and illustrates the intermetallic phase's extraction.

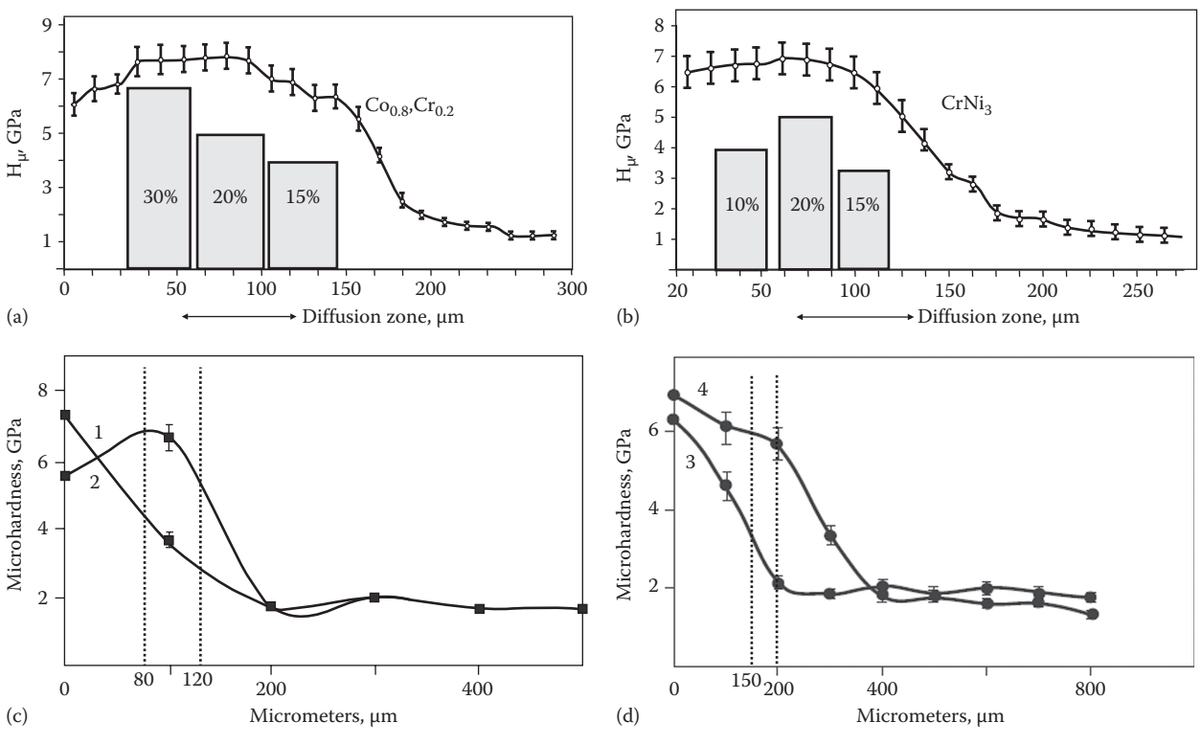

FIGURE 21 Microhardness Hμ distribution through the thickness from the surface. Volume fraction of the intermetallic phases are pointed for the coating, made of Co–Cr (a); for the coating, made of Ni–Cr (b). The results of Ni based coating microhardness test (cross section) Ni–Cr: 1–80 μm and 2–120 μm (c); 3–150 μm and 4–200 μm (d).

with different thickness from 80 to 200 μm (as deposited). For comparison, all the measurements were provided after deposition without additional melting by plasma jet. From these figures, we see that for all three coatings, maximal hardness (6.4 ÷ 7) GPa is obtained near the surface layer, but for coating with the thickness of 120 μm, hardness near the surface is lower and equals to 5.7 GPa, but when the depth is more than 80–100 μm, hardness increases and equals to 7 GPa. In other words, according to SEM data (with chemical composition microanalysis) and to XRD with TEM (phase composition analysis), in this case near the surface, we found great concentration of oxygen-carbide phases (so, this experiment seems to be not the most successful). Hardness of the steel substrate is 1.78 ± 0.11 GPa, Young modulus equals to 229 GPa. At the same time, Young modulus for Ni–Cr coating is 193 ± 15 GPa. We should mention that in Co–Cr coatings, microhardness maximum value is a little bit higher and equals to (7.5 ÷ 8) GPa.

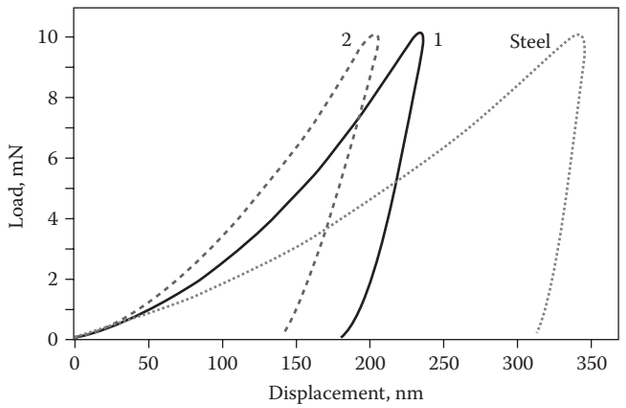

FIGURE 22 Loading and unloading curves obtained using a nanoindenter for the coating, which was deposited using high-velocity plasma jet: (1) coating as deposited; (2) after plasma jet melting with a melted layer thickness 45–50 μm.

Hardness of the transition layer between coating and substrate is (3.7 ÷ 3.9) GPa for samples with Co–Cr coatings, so in this case, hardness is two times greater than for steel substrate.

As it is seen from these results, near-surface layer melting by plasma jet leads to small increasing of hardness (experiments were provided on the polished surfaces with small 3° angle lap).

Loading and uploading curves for nanohardness indentation on the steel substrate are presented on Figure 22. Curve 1 corresponds to the as-deposited state; curve 2 corresponds to the state after subsequent plasma jet treatment (two passes, 5×10^6 W/cm^2).

Figure 22 shows curves of loading for the substrate and Co–Cr coating after melting by a high-velocity pulsed plasma jet.[25] These data indicate that the coating nanohardness is 8.7 GPa and substrate nanohardness is 3 GPa (the substrate elasticity modulus is about 210 GPa).

Nanohardness H, Young modulus E*, and H^3/E^{*2} ratio, which were calculated according to the obtained data for coatings before and after treatment by irradiation, is shown in Figure 23. Coefficient H^3/E^{*2} is proportional to the material resistance to plastic deformation.[11] We can conclude that plasma jet influence increases plasticity of the coatings and does not reduce its strength properties.

Results of the investigation of structural phase transformations in the coatings based on Ni–Cr and Co–Cr are presented. Such coatings were melted by an electron beam or impulse plasma flux under the computational regimes. The comparison of the structure and properties of the coatings was made before and after treatment by irradiation. Evolution of microstructure and phase composition of the coatings was analyzed, which was caused by irradiation heating.

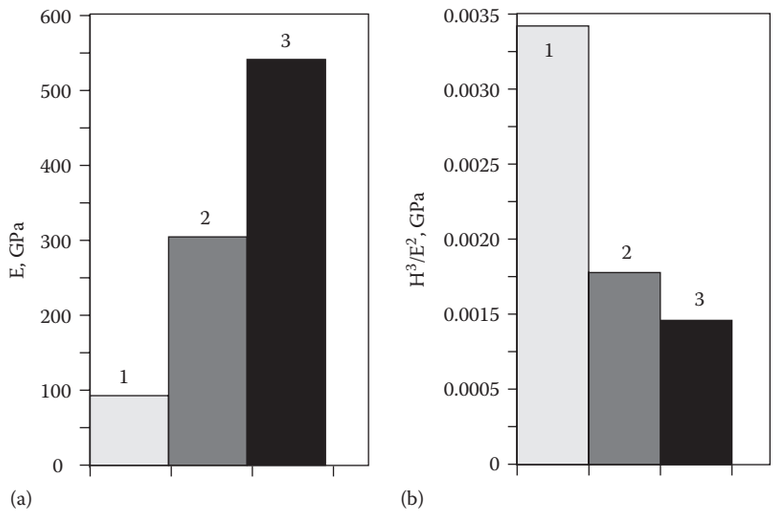

FIGURE 23 Comparison of the strength properties: E, GPa (a), H^3/E^*, GPa (b), of the modified coatings, made of (1) Ni–Cr, (2) Ni–Cr after treatment by plasma jet and substrate.

To evaluate parameters of relief roughness for Co–Cr coating surface after plasma jet melting, we have additionally used an optical microscope with laser attachment VEECO. As it can be observed from Figure 24a–c, red regions are protrusions of melted and deformed powder particles, dark-blue regions are valleys, and green regions are surface areas with very low roughness (plateau). The table inside the Figure 24a presents relief parameters obtained from the studied region (Rq, Ra, Rt, Rp, Rv).

In Table 6, we systemized all results devoted to detection of the coating's surface roughness in dependence on treatment (melting) regimes. It is obvious, that sizes of roughness in three dimensions decreases when plasma jet density increases on two orders, 30%–50% at the average (two passes of plasma jet). But our previous results indicate that increasing the number of plasma jet passes up to 10 decreases significantly the size of the roughness. But stresses in the coatings also increases in this case, and it can influence negatively on physical and mechanical properties and strength.

In our works,[43,47] we provided model experiments on treatment and melting of α-Fe samples and low carbon steel. We changed eroding electrode from Mo to Ti, then to W. We

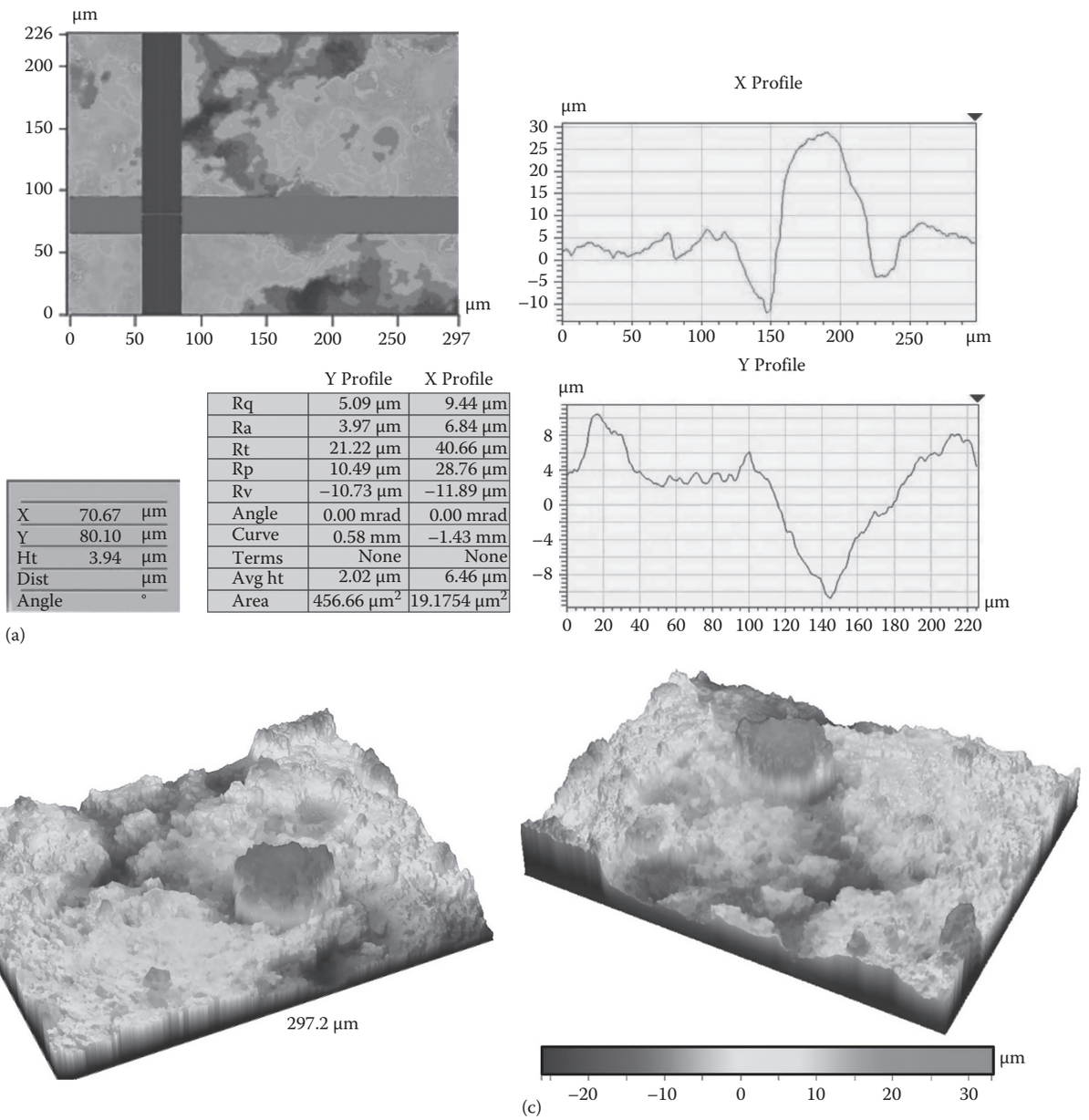

FIGURE 24 An image of Co–Cr coating region after its near-surface layer melting by a plasma jet: surface roughness diagram (dark-blue and red colors) (a); (b) a total view of selected coating region, 3D colored image; colored image for a region of 297.2 µm × 226.2 µm (c). To the right, we demonstrated a scale, which was painted in different colors according to the position of the coating surface interface from horizontal.

AQ8

TABLE 6
Influence of Plasma Jet Melting Regimes on Coating's Roughness

Coating	Rt, μm	Rp, μm	Power Density, W/cm²	Rv, μm	Comments
Ni–Cr	28.60	16.80	As deposited	31.50	After plasma treatment (two passes), Rt—width on x coordinate, Rp—width on y coordinate, Rv—height of roughness
	21.30	14.20	5×10^5	30.20	
	19.80	13.30	1×10^6	26.40	
	17.20	11.40	5×10^6	19.70	
Co–Cr	40.66	28.76	As deposited	50.20	
	38.20	26.37	5×10^5	47.40	
	32.30	22.80	1×10^6	42.30	
	28.54	17.12	5×10^6	37.50	
	26.57	14.38	7.8×10^6	29.80	

defined concentration of alloying element over the depth, and we explored thickness of melted layer by applying pressure to sample. Elementary composition analysis was done using RBS, PIXE, and EDS. We detected that, in the time of first pass, regions with very high Mo concentration (up to 80 at.%) are observed near the surface (if such element was used as doping or eroding electrode). After 2–4 passes (and more, up to 10 passes), we detected that Mo concentration equals to (10 ÷ 12) at.% near the surface, impurities are distributed regularly on the depth (10 ÷ 15) μm (RBS, proton beam energy 2.08 MeV), and Mo concentration on the depth more than 30 μm is near (1.1 ÷ 1.4) at.%, on the depth (40 ÷ 50) μm, barely 0.8 (in some cases). Depth of the melted layer equals to (40 ÷ 50) μm, it was detected from images of cross sections, which were obtained using metallography and SEM with backscattering electrons and using microanalysis over the depth with the help of EDX.[43,45–47] That is why we didn't provide such model experiments in this work and, due to the aforementioned, we state that the thickness of melted layer in Ni–Cr and Co–Cr coatings is the same one and equals (40 ÷ 50) μm.

Figure 25 shows the dependences between wear curves, obtained for initial coatings, and for those after pulsed plasma modification. From these dependences, one can see that the highest wear was observed in the stainless steel substrate. Plasma detonation deposition of powder coatings substantially decreases the wearing of a treated surface. Thermal hardening of the coating by pulsed plasma jet allows having the most optimum combination of hardness and plasticity.

The tests of sample surfaces for wear resistance in technical Vaseline medium demonstrated that

1. Deposition of powder coatings on cobalt base under the aforementioned regimes resulted in a 12-time increasing of their surface wear resistance in comparison with the substrate material.
2. Repeated HVPJ treatment of surfaces resulted in a 25-time wear decreasing (which was likely to be related to Mo oxide formation).

We have fabricated samples, made of stainless steel with Co–Cr coating, at elevated temperatures up to 80°C in aggressive environment (acidic environment). The corrosion potential (E_{corr}) in the case of the uncoated steel samples was found to be 457 mV (see Table 7) where a significant decrease was observed in the case of coated samples and after melting using plasma jet (without powder). The decrease of E_{corr} and the corrosion and passivation current density in the case of coated steel samples indicates an enhancement of corrosion

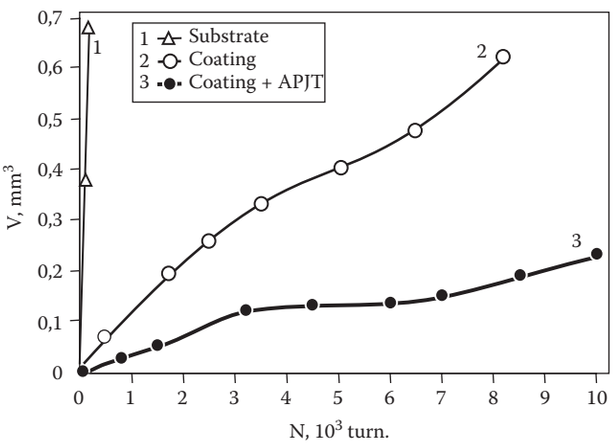

FIGURE 25 Dependence of surface wear for powder coatings based on cobalt during dry friction on the number of rotations: (1) the substrate material (stainless steel); (2) wearing of plasma detonation produced coatings (200 μm thick); (3) effect of coating surface melting as a result of pulsed plasma flow action (2 passes) on wear resistance.

TABLE 7
Parameters and Values of the Corrosion Tests

Parameter	Value
β_a	250.9e–3 V/decade
β_c	632.1e–3 V/decade
I_{corr}	1.880 μA
E_{corr}	–87.60 mV
Corrosion rate	6.883 μpy
Chi squared	3.772

TABLE 8
Results of the Corrosion Tests

Corrosion Stability Test Results in 3% NaCl Solution					
	Corrosion Potential	Corrosion Current	Passivation Current	Passivation Potential	Corrosion Velocity
	ϕ_{corr}, mV	$i_{corr,}$ μA	$i_{pass,}$ μA	$\phi_{pass,}$ mV	$V_{corr,}$ μm/year
Substrate	–490	5.20	2.00	1390	3.7
Coating made of Ni–Cr after treatment	–380	0.89	1.00	1170	2.2

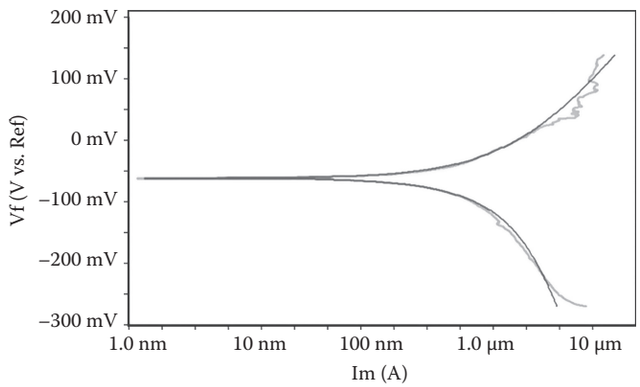

FIGURE 26 Experimental dependences for corrosion and Tafel curves for the sample Co–Cr.

resistance due to the protective action of the deposited (melted) layer. Good results were obtained for corrosion resistance in an abrasive medium, near 17 ÷ 22 times higher than the stainless steel substrate (see Table 8).

Samples covered with Co–Cr coatings had 6.8 and 8.4 μg/year corrosion rate; it depends on the composition of the thin layer (stoichiometry) (Figure 26 and Table 7).

Comparison of corrosion tests for Ni–Cr and Co–Cr coatings showed that under hard test's conditions (0.5 M H_2SO_4, ≈ 80°C), Ni–Cr coatings demonstrates much better characteristics, including elementary analysis (with AES and EDX) and nuclear reaction analysis. It will be discussed in detail in a separate chapter.

CONCLUSIONS

AQ10 Investigations of multiphasic coatings with intermetallic compounds, oxides, and carbides, after subsequent melting by plasma jet no less than two passes. Micro- and nanostructure crystallites appearing, intensification of diffusion and mass transfer processes on the borders of grains and phases, and, as a result, element's redistribution along the thickness are results of plasma jet influence.

As a result of this processes in the layer and fast cooling of the melts with thickness up to 50 μm, [43,44] partial amorphization of the coating parts is observed, local regions of nanograins with different crystallographic orientation are formed, and preferential crystallites growth take place (in other words, texture is formed) along the heat flow (or plasma jet) direction.

Structural phase transformations, changes in chemical composition of the coatings, and near-surface layer homogenization lead to significant changing of mechanical, tribotechnical, and corrosion properties. Long-term usage (5–7 years) of samples with Ni–Cr and Co–Cr coatings and finished manufactures with such coatings showed that their physical and mechanical characteristics are stable and do not change in the experiment error limits. Thus, we can say that such Ni–Cr and Co–Cr coatings (formed by deposition using pulse plasma detonation technology with subsequent plasma jet melting with power density up to 5×10^6 W/cm^2) may be perspective in different fields of science and techniques, for example, for protection and improvement of hydropower plants turbine blades and nuclear reactors walls in nuclear industry.

ACKNOWLEDGMENTS

This work was partly funded by FRSF-41/-020 from Ukraine, as well as by the Research Project 011U001382 "Designing of basis of formation of multicomponent nanostructured coatings with high physical and mechanical properties."

REFERENCES

1. Tyurin, Yu.N. and Pogrebnjak, A.D. Advances in the development of detonation technologies and equipment for coating deposition. *Surf. Coat. Technol.* 111(2–3) (1999): 269–276.
2. Pogrebnjak, A.D., Tyurin, Yu.N. Modification of material properties and coating deposition using plasma jets. *Phys. Usp.* 48(5) (2005): 487–514.
3. Boulos, M., Pfender, E. Materials processing with thermal plasmas. *MRS Bull.* 21(8) (1996): 65–68.
4. Pogrebnjak, A.D., Bratushka, S.N., Boyko, V.I., Shamanin, I.V., Tsvintarnaya, Yu.V. A review of mixing processes in Ta/Fe and Mo/Fe systems treated by high current electron beams. *Nucl. Instrum. Meth. B* 145 (1998): 373–390.
5. Pogrebnjak, A.D., Mikhaliov, A.D., Pogrebnjak, N.A. et al. Evolution of vacancy defects and dislocations in surface-layers of iron as a result of pulsed electron-beam treatment. *Phys. Lett. A* 241(6) (1998): 357–363.
6. Pogrebnjak, A.D., Bazyl', E.A. Certain features of high-dose and intensive implantation of Al ions in iron. *Vacuum* 64 (2002): 1–7.
7. Pogrebnjak, A.D., Lebed, A.G., Ivanov, Yu.F. Modification of single crystal stainless steel structure (Fe–Cr–Ni–Mn) by high-power ion beam. *Vacuum* 63(4) (2001): 483–486.

8. Pogrebnjak, A.D., Ruzimov, Sh.M., Alontseva, D.L. et al. Structure and properties of coatings on Ni base deposited using a plasma jet before and after electron a beam irradiation. *Vacuum* 81 (2007): 1243–1251.
9. Kadyrzhanov, K.K., Komarov, F.F., Pogrebnjak, A.D., Rusakov, V.S., Turkebaev, T.E. *Ion Beam and Ion-plasma Modification of Materials.* (in Russia) Moscow, Russia: Moscow State University, 2005.
10. Rykalin, N.N., Zuev, I.V., Uglov, A.A. *Fundamentals of Electron-Beam Treatment of Metals* (Russia), Moscow, Russia: Mashynostroenie, 1978, 457p.
11. Pogrebnjak, A.D., Vasiliuk, V.V., Alontseva, D.L. et al. Structure and properties of coatings of nickel alloy after electron beam melting. *Tech. Phys. Lett*. 30(4) (2004): 78–86.
12. Alontseva, D.L., Bratushka, S.N., Borysenko, A.A., Drobyshevska, A.A., Kulik, I.A., Prokhorenkova, N.V., Pshyk, A.V., Rogoz, V.N. Formation of micro- and nanostructured phases in coatings based on Ni–Cr and Co–Cr, their structure and properties. *Metallofizika i Noveishie Tekhnologii* 33(6) (2011): 721–745.
13. Alontseva, D.L., Bratushka, S.N., Il'yashenko, M.V. et al. Formation of stable nanostructured phases in plasma-jet-treated Ni–Cr powder coatings. *Phys. Metals Metallogr.* 113(8) (2012): 785–794.
14. Pogrebnjak, A.D., Il'yashenko, M.V., Kshnyakin, V.S., Tyurin, Yu.N., Ivanov, Yu.F. The structure and properties of a hard alloy coating deposited by high-velocity pulsed plasma jet onto a copper substrate. *Tech. Phys. Lett*. 27(9) (2001): 749–751.
15. Pogrebnjak, A.D., Shumakova, N.I. Effect of "duplex" treatment of changes of physical and mechanical properties of steel (0.3 wt% C). *Surf. Coat. Technol*. 122 (1999): 183–187.
16. Pogrebnjak, A.D., Lozovan, A.A., Kirik, G.V., Shytov, N., Stadnik, A.D., Bratushka, S.N. *Structure and Properties of Nanocomposite, Hybrid and Polymer Coatings.* (in Russia) Moscow, Russia: Publisher USSR, 2011.
17. Azarenkov, N.A., Beresnev, V.M., Pogrebnjak, A.D. *Structure and Properties of Protective Coatings and Modified Layers.* (in Russia) Kharkov, Ukraine: Kharkov National University, 2007.
18. Pogrebnjak, A.D., Shpak, A.D., Beresnev, V.M. Structure and properties of protective composite coatings and modified surface prior and after plasma high energy jet, in *The New Nanotechniques*, eds. A. Malik and R.J. Rawat (Nova Science Publishers, New York, 2009), pp. 21–114.
19. Ivasishin, O.M., Pogrebnjak, A.D., Bratushka, S.N. *Nanostructured Layers and Coatings Formed by Ion-Plasma Fluxes in Titanium Alloys and Steels.* Kiev, Ukarine: Academperiodika, 2011.
20. Pogrebnjak, A.D., Danilionok, M.M., Uglov, V.V. et al. Nanocomposite protective coatings based on Ti–N–Cr/Ni–Cr–B–Si–Fe, their structure and properties. *Vacuum* 83 (2009): 235–239.
21. Alontseva, D.L., Pogrebnjak, A.D., Prohorenkova, N.V., Kaverin, M.V. Nanostructure formation in the nickel-chrome coating after duplex threatment. *J. Nano-Electron. Phys*. 2 (2010): 12–28.
22. Ivanov, L. I., Platov, Yu. M. *Radiation Physics of Metals and Its Applications.* Cambridge, U.K.: Cambridge International Science Publishing, 2004.
23. Pogrebnyak, A.D., Ilyashenko, M.V., Kulment'eva, O.P. et al. Structure and properties of a hard alloy deposited on a copper substrate by means of a pulsed plasma spray technology. *Tech. Phys.* 46(7) (2001): 897–904.
24. Pogrebnyak, A. D., Il'yashenko, M.V., Kshnyakin, V.S. et al. The structure and properties of a Cr_3C_2–Ni coating deposited by a high-velocity plasma jet onto a copper substrate. *Tech. Phys. Lett*. 29(12) (2003): 1028–1030.
25. Thorpe, M.L., Richter, H.J. A pragmatic analysis and comparison of the ASM International HVOF process. In *The Proceedings of the International Thermal Spray Conference & Exposition*, Orlando, FL, May 28–June 5, 1992, pp. 137–148.
26. Bhagat, R.B., Amateau, M.F., Papyrin, A. et al. Deposition of nickel aluminum bronze powder by cold gas dynamic spray method on 2618 for developing wear resistant coatings. In *Proceedings 10th National Thermal Spray Conference on Thermal Spray: A United Forum for Scientific and Technological Advances*, ASM International, 1997, pp. 361–367. AQ11
27. Wielage, B., Rupprecht, C., Paczkowski, G. et al. A new way in HVOF technology—CFD optimized TOPGUN®AIRJET for powder and wire. In *The Proceedings of ITSC 2008*, Maastricht, the Netherlands 2008, pp. 145–150.
28. Chivavibul, P., Watanabe, M., Kuroda, S. et al. Development of WC-Co coatings deposited by warm spray process. In *The Proceedings of ITSC 2008*, Maastricht, the Netherlands, 2008, pp. 64–69.
29. Korobov, Y., Filippov, M. HVAF coating application in steel-making process. In *The Proceedings of ITSC 2008*, Maastricht, the Netherlands, 2008, pp. 1362–1365.
30. Blose, R., Roemer, T., Nichols, R., Mayer, A., Beatty, D.E. Automated cold spray system: Description of equipment and performance data. In *The Proceedings of ITSC 2005*, Basel, Switzerland, 2005, pp. 56–64.
31. Hoell, D.E., Richter, P. KINETIKS@4000—New perspective with cold spraying. In *The Proceedings of ITSC 2008*, Maastricht, the Netherlands, 2008, pp. 477–478.
32. Jodoin, P., Richer, P., Yandouzi, M., Erdi, A., Pulsed-cold gas dynamic spraying process: Development and capabilities. In *The Proceedings of ITSC 2007*, Beijing, China, 2007, pp. 19–24.
33. Kitamura, J., Sato, K., Aoki, I. et al. Mechanical properties of WC/Co coatings prepared by cold spraying. In *The Proceedings of ITSC 2008*, Maastricht, the Netherlands, 2008, pp. 110–114.
34. Parco, I., Barykin, I., Fagoaga, I., Vaquero, C. Development of wear resistant ceramic coatings by HFPD. In *The Proceedings of ITSC 2008*, Maastricht, the Netherlands, 2008, pp. 140–144.
35. Zhong, M., Liu, W., Yao, W. et al. Microstructural evolution in high power laser cladding of stellite 6+WC layers. *Surf. Coat. Technol*. 157(2–3) (2002): 128–137.
36. Malayoglu, U., Neville., U. Comparing the performance of HIPed and cast stellite 6 alloy in liquid-solid slurries. *Wear* 255(1–2) (2003): 181–194.
37. Birol, Y. High temperature sliding wear behaviour of Inconel 617 and Stellite 6 alloys. *Wear* 269(9–10) (2010): 664–671.
38. Tyurin, Yu. N., Kolisnichenko, O.V. Plasma-detonation technology for modification of the surface layer of metal parts. *Open Surf. Sci. J.* 1 (2009): 13–19.
39. Gorelik, S.S., Rastorguyev, L.N., Skakov, Yu.A. *X-Ray and Electron Optic Analysis.* (in Russia) Moscow, Russia: MISIS, 1994.
40. Oliver, W.C., Pharr, G.M. An improved technique for determining hardness and elastic modulus using load and displacement sensing indentation experiments. *J. Matter. Res*. 7(6) (1992): 1564–1583.
41. Ageev, N.V., Petrov, L.A. Ed. *State Diagrams of Metallic Systems* (Russia), Moscow, Russia, 1985, pp. 60–62. AQ12

42. Pogrebnjak, A.D., Kobzev, A.P., Gritsenko, B.P. et al. Effect of Fe and Zr ion implantation and high-current electron irradiation treatment on chemical and mechanical properties of Ti–V–Al Alloy. *J Appl. Phys.* 87(5) (2000): 2142–2148.
43. Bratushka, S.N., Tyurin, Yu.N., Kolisnichenko, O. V. et al. Structure and tribological characteristics of steel under melting by plasma flow and simultaneous Mo and W alloying. *J. Frict. Wear* 33(1) (2012): 22–33.
44. Pogrebnjak, A.D., Beresnev, V.M., Kaverina, A.Sh. et al. Adhesive strength and physical, mechanical, and triboengineering properties of nano- and microstructural Al_2O_3 coatings. *J. Frict. Wear* 33(1) (2012): 195–202.
45. Zou, J.X., Grosdidier, T., Zhang, K.M., Dong, C. Mechanisms of nanostructure and metasable phase formations in the surface melted layer of HCPEB treated D2 steel. *Acta Mater.* 54 (2006): 5409–5419.
46. Zou, J.X., Grosdidier, T., Zhang, K.M., Dong, C. Cross-sectional analysis of the graded structure in an AISI D2 steel treated with low energy high current pulsed electron beam. *Appl. Surf. Sci*. 255 (2009): 4758–4764.
47. Alontseva, D.L. Structural-phase state and properties of Ni–Cr, Co–Cr, Fe–Ni–Cr alloys in the results of impact of the concentrated energy flows. The thesis abstract for the degree of Doctor of Physical and Mathematical Sciences (Dr. Sci.). Barnaul, Russia, 2012.
48. Alontseva, D., Pogrebnjak, A., Kolesnikova, T., Russakova, A. Modeling of process in Co-based coating exposed to plasma irradiation. *Mater. Sci.* (Medziagotyra) 19 (2013): 277. AQ13
49. Alontseva, D.L. The study of using plasma techniques for deposition of Ni–Cr based coating on steel substrate and modification of their properties by duplex treatment. *Przeglad Elektrotechniczny* 87(7) (2007): 42–44.
50. Alontseva, D., Misserva, S., Russakova, A. Characteristics of structure and properties of plasma-detonated Ni–Cr and Co–Cr based powder alloys coating. *J. Mater. Sci. Eng.* A3(1) (2013): 41–49.
51. Bratushka, S.N., Kolisnichenko, O.V., Mikhalev, A.D. et al. Formation ultradispersed surface layers of the steel after doping with ions of metal in the mode of melting plasma jet. *Metallofiz. Noveishie Tekhnol.* 35(9) (2013): 1251–1270.

AUTHOR QUERIES

[AQ1] Please check if identified all heading levels are okay.
[AQ2] Please check if edit to sentence starting "However, according to…" is okay.
[AQ3] Please provide specific details referred by the term "above" in this sentence.
[AQ4] Please provide appropriate in-text citation for Table 3.
[AQ5] Please confirm if "He^{4}_{+2}" should be changed to "He_{4}^{+2}" in the caption of Figure 4.
[AQ6] Paragraph starting "Coating surface…" has been used twice in the text. Please check if one needs to be deleted.
[AQ7] Please check if edit to sentence starting "Coatings, based on…" is okay.
[AQ8] Figure 24 will be printed in grayscale. Please rephrase mention of color.
[AQ9] The term "enhanceable" has been changed to "elevated." Please check if okay.
[AQ10] Please check sentence starting "Investigations of multiphasic…" for clarity.
[AQ11] Please provide location for Ref. [26].
[AQ12] Please provide publisher name for Ref. [41].
[AQ13] Please cite Refs. [48–51] in text.